Solid Earth
Discussions

Open Access

EGU

Fault zone architecture of a large plate-bounding strike-slip fault: a case study from the Alpine Fault, New Zealand

Bernhard Schuck[1], Anja M. Schleicher[2], Christoph Janssen[1], Virginia G. Toy[3], and Georg Dresen[1,4]

[1]Helmholtz Centre Potsdam, GFZ German Research Centre for Geosciences, Section 4.2: Geomechanics and Scientific Drilling, Potsdam, Germany
[2]Helmholtz Centre Potsdam, GFZ German Research Centre for Geosciences, Section 3.1: Inorganic and Isotope Geochemistry
[3]Department of Geology, University of Otago, Dunedin, New Zealand
[4]University of Potsdam, Institute of Geosciences, Potsdam Germany

Correspondence: Bernhard Schuck (bernhard.schuck@gfz-potsdam.de)

Abstract. New Zealand's Alpine Fault is a large, plate-bounding strike-slip fault, that ruptures in large ($M_W > 8$) earthquakes. Its hazard potential is linked to its geometrical properties. We conducted field and laboratory analyses of fault rocks to elucidate their influence on its fault zone architecture. Results reveal that the Alpine Fault zone has a complex geometry, comprising an anastomosing network of multiple slip planes that have accommodated different amounts of displacement. Within it, slip

5   zone width is demonstrably not related to lithological differences of quartzofeldspathic lithologies, which vary slightly along-strike. The young, largely unconsolidated sediments that constitute the footwall in some outcrops have a much more significant influence on fault gouge rheological properties and structure. Additionally, seismic investigations indicate that the exposed complex fault zone architecture extends into the basement. This study reveals the Alpine Fault contains multiple slip zones surrounded by a broader damage zone; properties elsewhere associated with carbonate or phyllosilicate-rich faults.

10

1   Introduction

A fault, a planar discontinuity in rock where one side has moved relative to the other parallel to the discontinuity plane, constitutes a rheological and mechanical manifestation of localized deformation (Twiss and Moores, 2007; Ben-Zion, 2008; Fossen, 2016; Fossen and Cavalcante, 2017). Many large faults zones are composed of networks of smaller, individual, but

15   related and interacting faults of self-similar geometry (Ben-Zion and Sammis, 2003; Twiss and Moores, 2007; Peacock et al., 2016). The structure, composition, hydrological properties and seismo-mechanical behavior of faults are typically intimately related. These interactions also govern strain distribution and depend on various factors, such as lithology (Faulkner et al., 2003; Schleicher et al., 2010; Holdsworth et al., 2011; Rybacki et al., 2011), fluid pressure (Hickman et al., 1995; Janssen et al., 1998; Fagereng et al., 2010) and stress field and stress magnitudes (Sibson, 1985; Faulkner et al., 2006; Lindsey et al.,

20   2014).

Faults control the strength of the Earth's lithosphere (Townend and Zoback, 2000; Bürgman and Dresen, 2008) and govern substantially fluid flow (Caine et al., 1996; Wibberley et al., 2008). Hydrocarbon production from fault-compartmentalized reservoirs (Van Eijs et al., 2006), exploitation of fault-hosted mineral deposits (Cox et al., 1986) and long-term integrity of potential nuclear waste repositories (Laurich et al., 2018) are practical examples demonstrating how important it is to

25 understand fault zone properties and their spatial and temporal evolution. Furthermore, large, plate-bounding strike-slip faults such as the Alpine Fault (New Zealand), the North Anatolian Fault Zone (Turkey) or the San Andreas Fault (USA) rupture in large ($M_W > 7$) earthquakes (Toppozada et al., 2002; Sutherland et al., 2007; Bohnhoff et al., 2016). Many of these faults are located in densely populated areas so they pose a significant geohazard (Eguchi et al., 1998; Sahin and Tari, 2000; Martínez-Garzón et al., 2015). Thus, from a georesource, seismic hazard and risk perspective, it is important to characterize the seismo-

30 mechanical properties of faults (Aksu et al., 2000; Zoback et al., 2007; Hollingsworth et al., 2017).

Caine et al. (1996) presented a conceptual model of the structure of fault zones that has three primary components (Fig. 1a). The protolith (I) hosts a damage zone (II) that is characterized by a fracture density significantly higher than the background values of the surrounding host rock (Chester et al., 1993; Biegel and Sammis, 2004; Faulkner et al., 2010). The damage zone contains the fault core (III) where most of the displacement has been accommodated (Caine et al., 1996). This conceptual

35 framework has been found to be applicable to faults across the full range of natural and experimental spatial scales (Anders and Wiltschko, 1994). Biegel and Sammis (2004) suggested a fault core should be defined as the zone within a fault where strain leads to granulation of rocks, distinct from a damage zone within which fracture density is high but fracturing has "not [been] sufficient to produce distinct particles". A fault core can be structurally and lithologically heterogeneous, and most of the displacement it accommodated may be localized along one or more principal slip zones (PSZ) defined by ultracataclasites or

40 fault gouges (Sibson, 2003; Janssen et al., 2014; Toy et al., 2015). Although most commonly less than 10 cm thick, PSZs may be up to 1 m thick (Sibson, 2003) and thicknesses tend to increase with increasing displacement (Evans, 1990; Faulkner et al., 2010; Ben-Zion and Sammis, 2003, and references therein). In general, fault zone thicknesses may range from millimeters (e.g. Antonellini and Aydin, 1994) to a few hundreds of meters (e.g. Bruhn et al., 1994).

The Punchbowl Fault, an inactive, exhumed part of the San Andreas Fault system, typifies this conceptual model of fault

45 zone architecture. It has a single PSZ embedded in a fault core and surrounding damage zone. A single, continuous gouge layer with 30 cm thickness on average, hosts the ~1 mm thick PSZ. The core of the Punchbowl Fault is surrounded by an approximately 15 m thick damage zone (Chester and Logan, 1986; Chester et al., 2005).

However, other faults show a more complex structure with changing properties along strike or down dip (e.g. Wibberley et al., 2008; Faulkner et al., 2010). For example, detailed studies of the Carboneras Fault, Spain, yielded a conceptual model

50 that is suitable for broader, typically phyllosilicate-rich fault zones, which tend to contain multiple high-strain zones (Fig. 1b; Faulkner et al. 2003). The Carboneras Fault is a predominantly strike-slip structure, that comprises an ~1 km thick tabular zone of continuous and anastomosing strands of phyllosilicate-rich fault gouge containing lenses of fractured protolith surrounded by an approximately 100 m wide damage zone. Scaly clays, which typically contain anastomosing shear planes, are examples of this distributed fault zone model on the hand-specimen scale (Vannucchi et al., 2003; Laurich et al., 2017).
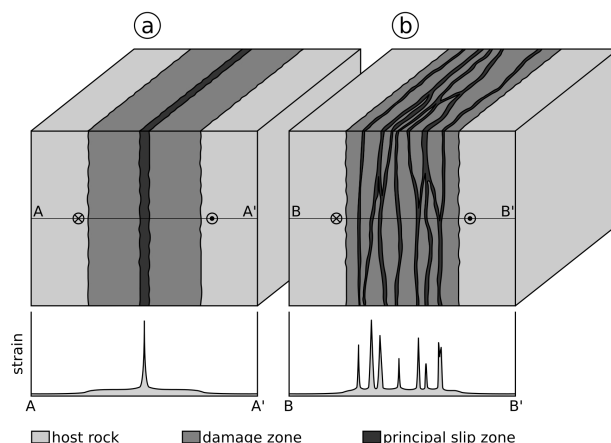
Figure 1. Conceptual end-member models of fault zone architecture. **(a)** According to the model of Caine et al. (1996) a fault is a relatively simple structure, where most of the strain is accommodated at a single, quite narrow fault core hosting a principal slip zone. **(b)** Faults being described by the model of Faulkner et al. (2003) are more complex and consist of a damage zone hosting multiple, anastomosing principal slip zones forming a complex network.

The fault zone architecture of New Zealand's Alpine Fault, a large, transpressional plate-bounding fault and a significant geohazard, has attracted increasing attention in the last ten years (e.g. Barth et al., 2012; Sutherland et al., 2012; Barth et al., 2013; Toy et al., 2015; Williams et al., 2016; Townend et al., 2017; Lukács et al., 2018; Schuck et al., 2018; Williams et al., 2018). Here, by combining results of these previous studies on the Alpine Fault's structure with new field observations, microstructural, mineralogical and geochemical analyses we show that the Alpine Fault has a complex fault geometry at and above seismogenic depths. Atypical for fault zones hosted in quartzofeldspathic protoliths, this complexity is not a function of lithology and implies that the Alpine Fault does not fit the classical models of fault zone architecture.

2 Geological Setting

2.1 The Alpine Fault and associated hazard

The Alpine Fault localizes most of the deformation associated with the relative displacement between the Australian Plate and the Pacific Plate. The fault is dominantly transpressive and runs through the South Island of New Zealand. The straight, 800 km long surface trace extends from Milford Sound in the SW to Hokitika in the NE, where it transfers displacement onto the four main fault strands of the Marlborough Fault System (the Wairau, Awatare, Clarence and Hope Faults; Fig. 2a). The Alpine Fault maintains a constant NE-SW strike for its entire length, but the fault dip changes from 80-90° SE SW of the Dun Mountain Ophiolite Belt (DMOB) to 30-50° SE in the central segment (Barth et al., 2013). The shallowest 1-2 km of the fault NE of Haast display northerly-striking oblique thrust sections and easterly-striking dextral strike slip sections of 1-10 km length (Norris and Cooper, 1995; Barth et al., 2012).

A 470 km right-lateral offset of the DOMB defines the minimum cumulative displacement along the fault. Displacement-normal shortening is on the order of 90 ± 20 km (Little et al., 2005). Strike-slip displacement rates are between 21 mm yr^{-1} and 29 ± 6 mm yr^{-1} (Norris and Cooper, 2000) corresponding to 60-80 % of the total relative velocity between the bounding plates

75 (DeMets et al., 2010). Seismic investigations indicate a maximum exhumation of ~35 km from a deep crustal, subhorizontal, NE-dipping detachment (Stern et al., 2001; Little et al., 2005). Long-term exhumation rates of 6-9 mm yr^{-1} are inferred from ^{40}Ar/^{39}Ar ages encountered between Franz Josef Glacier and Fox Glacier (Little et al., 2005). A combination of these high exhumation rates and meteoric fluid circulation driven by steep topographic gradients results in a very high geothermal gradient of up to 125 °C km^{-1} encountered in valleys (Menzies et al., 2016; Sutherland et al., 2017).

80 Currently, the Alpine Fault does not exhibit creep and is thought to be seismically locked to a depth of 12-18 km (Beavan et al., 2007). It is known to rupture in large earthquakes ($M_W > 8$), while generating up to 8-9 m of lateral and up to 1 m of normal displacement (Sutherland et al., 2007; Nicol et al., 2016). While events like the most recent one in 1717 AD might rupture the entire fault, differing recurrence intervals of 263 ± 68 years for the central segment and 291 ± 23 years for the southern segment demonstrate that individual sections of the fault might fail independently (Fig. 2a; Sutherland et al. 2007;

85 Howarth et al. 2018 and references therein). Considering the potential to produce large magnitude earthquakes and the time passed since the last event, the Alpine Fault is late in its seismic cycle and thus constitutes one of the South Island's major geohazards.

2.2 Lithology

The Australian Plate footwall assemblage encompasses Paleozoic to Cretaceous plutonic rocks intruded into metasediments

90 (Fig. 2b). As these units are mostly overlain by Quaternary fluvioglacial sediments, footwall rocks are poorly exposed (e.g. Toy et al., 2015). In the Pacific Plate hanging-wall, a narrow, 12-25 km wide, elongate belt of metamorphosed sediments, the Alpine Schist, is exposed from SW of Jackson Bay to the fault's north-eastern termination (e.g. Sibson et al., 1979; Grapes and Watanabe, 1992; Scott et al., 2015). The Alpine Schist originates mostly from the Torlesse Terrane. This terrane is a polygenetic metamorphic suite with the Alpine Schist being its high-grade, and most recently-formed part (Roser and Cooper, 1990). The

95 amphibolite-greenschist facies rocks of the Alpine Schist have dominantly metapelitic to metapsamitic compositions, with rare metabasite and metachert. Metamorphic grade decreases from K-feldspar and oligoclase amphibolite facies through garnet, biotite and chlorite greenschist facies to pumpellyite-actinolite and prehnite-pumpellyite facies with increasing SE-distance from the fault plane (e.g. Grapes and Watanabe, 1992; Scott et al., 2015). However, a combination of significant right-lateral displacement and high-exhumation rates resulted in 200-300 m wide inverted metamorphic sequences cropping out structurally

100 above brittle fault rocks in the central segment (Cooper and Norris, 2011). Irrespective of local variations, typical mineral phases encountered in Alpine Schist-derived fault rocks are quartz, feldspar, garnet, muscovite, biotite, other minor phases and, in case of metabasites, hornblende and epidote (Norris and Cooper, 2007). At the Waikukupa Thrust there are remnants of highly disrupted, intensely strained and sheared granite pegmatites indicating simple shear strains of more than 150 and coeval pure shear stretches of ~3.5 (Norris and Cooper, 2003; Toy et al., 2013).
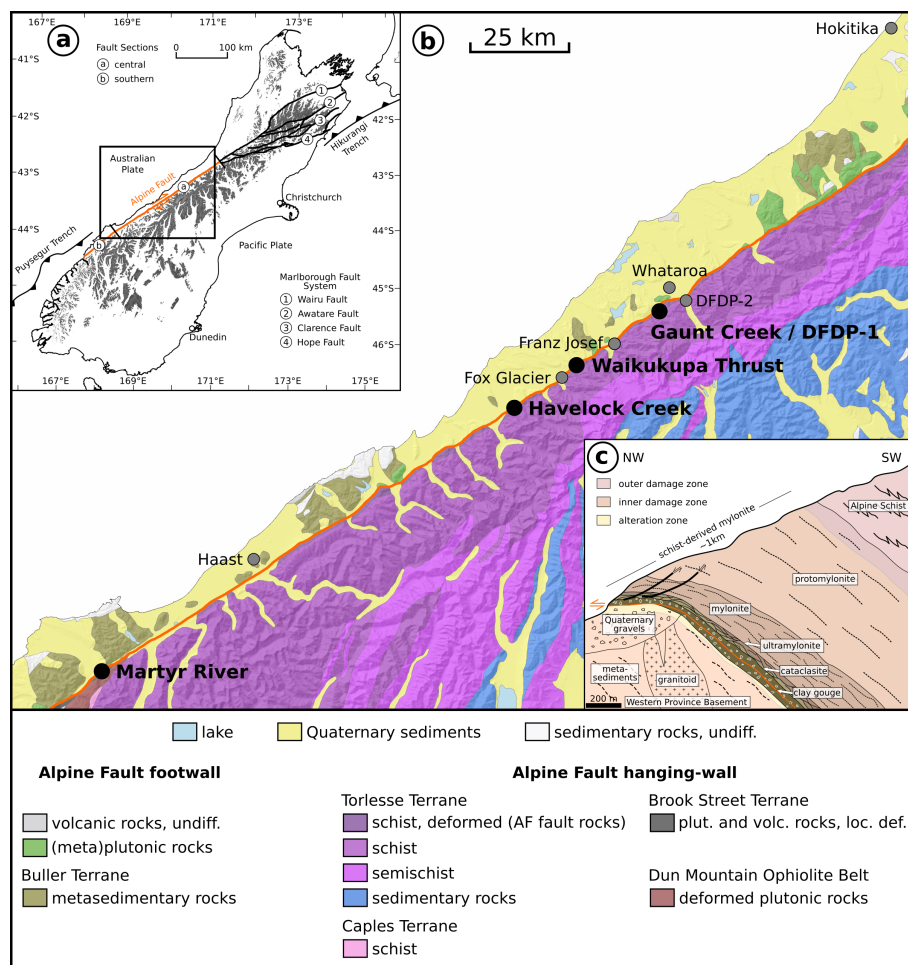
Figure 2. (a) Plate tectonic setting of New Zealand's South Island with the Alpine Fault's onshore segment being highlighted in orange. Position of (b) is indicated by black box. **(b)** Simplified geological map of the study area. Alpine Fault trace shown in orange. Locations of investigated outcrops are highlighted in bold font. Map is based on the geological map of New Zealand's South Island (Edbrooke et al., 2015) and the digital elevation model of Columbus et al. (2011). **(c)** Typical shallow-depth sequence of Alpine Fault rocks. Figure was modified from Norris and Cooper (2007). Extents of alteration zone were derived from Sutherland et al. (2012) and extents of inner and outer damage zone from Townend et al. (2017).

105　　Whereas the Alpine Schist constitutes the protolith of fault rocks in the central portion of the Alpine Fault, a comparatively small (~550 m thick) sliver of the Brook Street Terrane (BST) is the protolith of samples from the southern segment (Fig. 2b). The sliver is surrounded by the DMOB and bound to the NE by the Alpine Fault. The BST is the remnant of a Permian island-arc system, mainly composed of basaltic to andesitic volcaniclastic and sedimentary rocks of prehnite to pumpellyite and locally greenschist metamorphic grade (Spandler et al., 2005).

2.3   Fault rocks of the Alpine Fault

Exhumation from deep-crustal levels resulted in the formation of an approximately one kilometer wide characteristic sequence of hanging-wall fault rocks (e.g. Reed, 1964; Sibson et al., 1979; Cooper and Norris, 2011; Toy et al., 2015, Fig. 2c). Progressive north-westward-increasing shear strain of the Alpine Schist yielded proto- to ultramylonites that are overprinted by a cataclastic fault zone displaying increasing damage towards the PSZ (Williams et al., 2016). Cataclastic shears in the ultramylonites are filled with phyllosilicates and exhibit strike-slip, normal and reverse kinematics. Cataclasites are composed of comminuted mylonite fragments within a matrix of pulverized host rock, authigenic chlorite, muscovite and illite (Sibson et al., 1979; Norris and Cooper, 2007; Boulton et al., 2012). Intense chloritization imparted a typical pale-green color to these 10-30 m wide cataclasites (Warr and Cox, 2001), which are cemented by authigenic phases, dominantly phyllosilicates and carbonates (Sutherland et al., 2012; Toy et al., 2015; Williams et al., 2016). The fault's PSZ is an incohesive and fine-grained gouge up to ~50 cm in thickness (Norris and Cooper, 2007; Boulton et al., 2012). Authigenic phyllosilicates cement the PSZ converting it into an impermeable hydraulic barrier preventing cross-fault fluid flow (Sutherland et al., 2012; Menzies et al., 2016). There is no location providing a continuous section from hard-rock hanging- to hard-rock footwall (Townend et al., 2009).
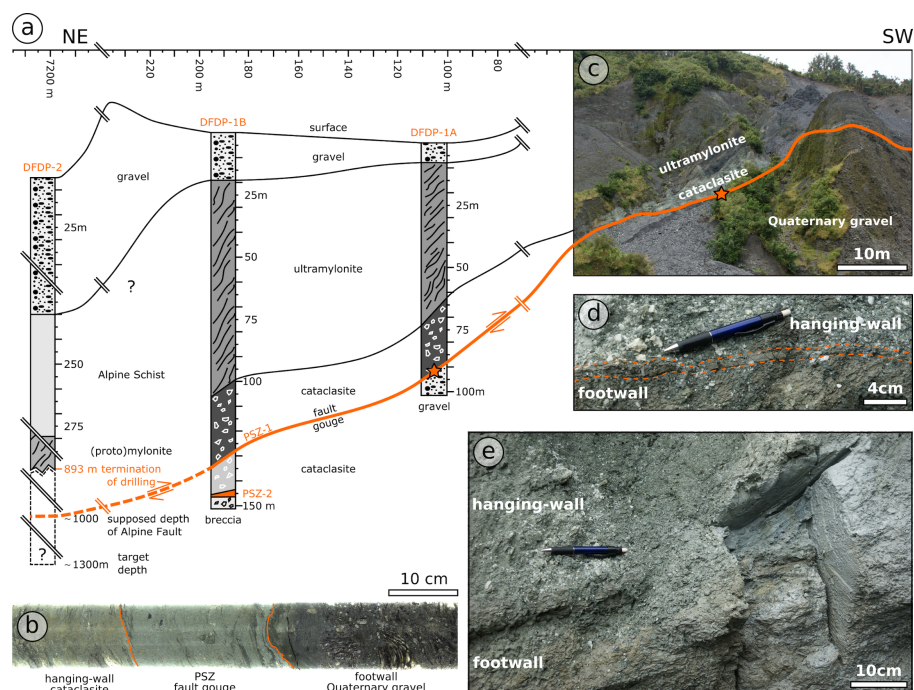
2.4   The Deep Fault Drilling Project

Studying the physical character of tectonic deformation at depth within a continental fault late in its interseismic period provided the motivation for the Deep Fault Drilling Project (DFDP, Fig. 3a, Townend et al., 2009). Phase 1 drilled two ~100 m (DFDP-1A) and ~150 m (DFDP-1B) deep pilot holes in January 2011 (Sutherland et al., 2012; Toy et al., 2015). These DFDP-1 boreholes provide a continuous section of fault rocks from hanging-wall ultramylonites to footwall gravels enabling lithological (Toy et al., 2015), mineralogical (Schleicher et al., 2015), geomechanical (Boulton et al., 2014; Carpenter et al., 2014) and geophysical analysis (Sutherland et al., 2012; Townend et al., 2013). In total, three ~20 cm thick PSZs were encountered. In DFDP-1A the PSZ is located between 90.67 and 90.87 m depth (Figs. 3a & b), and in DFDP-1B two PSZs were encountered at 128.30-128.50 m and 143.96-144.16 m depth, respectively (Fig. 3a, Toy et al., 2015).

Another two boreholes were drilled in DFDP phase 2 (DFDP-2A: 212.6 m MD - measured depth, DFDP-2B: 893.1 m MD) about 7.5 km ENE of the location of DFDP-1 (Fig. 2b, Toy et al., 2017). Phase 2 yielded cuttings for petrographic investigations (Toy et al., 2017) and provided various insights into fault zone architecture by wireline logs (e.g. Janku-Capova et al., 2018; Massiot et al., 2018) but was not able to penetrate and sample the fault core due to scientific and technical difficulties (Toy et al., 2017). DFDP boreholes from both phases provide the opportunities for long-term monitoring of the Alpine Fault (e.g. Sutherland et al., 2015).

2.5   Study locations

For this study, all known outcrops with accessible PSZ between Martyr River in the SW and Kokatahi River, SSE of Hokitika in the NE were investigated ~~in the austral summer 2015/16~~ (Fig. 2b). Furthermore, cataclasite and fault gouge samples were available from the DFDP-1A core. Four of the five investigated locations, Havelock Creek, Waikukupa Thrust, Gaunt Creek

Figure 3. (a) Schematic overview of Deep Fault Drilling Project (DFDP) boreholes drilled in phase 1 at Gaunt Creek and phase 2 within the Whataroa River Valley. Star at DFDP-1A indicates location of b. **(b)** Segment of 180° scan of PSZ encountered at DFDP-1A drill core (run 66, section1). **(c)** Individual fault rock units of the Alpine Fault zone are well-recognizable at the outcrop Gaunt Creek, in close proximity to the DFDP boreholes. Star indicates location of d and e. **(d)** An approximately 1 cm thick, brown layer indicated by stippled orange lines, was interpreted to represent the PSZ at Gaunt Creek. **(e)** Sample location (specimen shown in figure 5b) some 10s of centimeter SW of location shown in d. Figure modified according to Sutherland et al. (2012) and Boulton et al. (2014).

and the core of DFDP-1A, are in the central segment of the Alpine Fault with the Alpine Schist as hanging-wall host rock. Rocks of the BST constitute the host of fault rocks encountered at Martyr River, the fifth and southwestern-most location. All outcrops are located along river banks providing good outcrop conditions.

145 Waikukupa Thrust is the only studied site that is considered to be inactive. Incision of the Waikukupa River resulted in a geomechanically unfavorable geometry leading to the abandonment of this thrust segment and re-localization of deformation approximately 700 m to the NE at Hare Mare Creek (Norris and Cooper, 1997).

3 Methods

3.1 Sampling

150 Fault rocks at Martyr River and Havelock Creek were sampled using hammer and chisel. At Waikukupa Thrust and Gaunt Creek samples were recovered using a hand-held chainsaw equipped with a silicon-carbide chain. After recovery, all outcrop

samples were immediately wrapped in aluminum and plastic foil to slow down drying. This procedure allowed continuous transects across the PSZ, which juxtapose hanging-wall cataclasites and footwall gravels, to be sampled from Martyr River and Waikukupa Thrust. However, the samples broke apart along the PSZ during shipping. An intact contact of PSZ on footwalls

155 material was only preserved from Gaunt Creek.

In summary, hanging-wall fault rocks are available from Martyr River, Waikukupa Thrust and DFDP-1A. PSZ samples originate from all five locations and footwall rocks were taken at Martyr River, Waikukupa Thrust and Gaunt Creek.

3.2 Microstructural analysis

Samples from Martyr River, Waikukupa Thrust and Gaunt Creek were cut dry with a low-speed saw perpendicular and parallel
160 to the fault trace. From all locations, subsamples were selected for microstructural analyses and subsequently embedded in resin prior to the preparation of 29 dry-polished thin sections using otherwise standard techniques.

Microstructural investigations were conducted using optical microscopy, scanning electron microscopy (SEM), transmission electron microscopy (TEM) and cathodoluminescence analyses (CL). Thin sections were studied with a Leica DM RX optical microscope and a FEI Quanta 3D SEM with focused ion beam (FIB; dual-beam machine). The SEM, equipped with a field
165 emission gun, operated at 20 kV in backscatter electron mode (BSE) and allowed semi-quantitative geochemical analyses with its EDAX energy dispersive X-ray analyzer (EDX). For TEM analyses, a platinum strip was deposited on the sites selected with the FIB of the SEM to enable subsequent preparation of 14 thin foils ($10 \times 8 \times 0.15$ µm) with a FEI FIB 200 following the procedure outlined by (Wirth, 2004, 2009). A FEI Tecnai G2 F20 X-Twin TEM with Gatan Tidiem energy filter, Fishione high-angle annular dark field detector (HAADF) and EDX operated at 200 kV and allowed nanoscale investigations. Cathodo-
170 luminescence analyses on calcite veins and cement were performed on thin sections using an Olympus polarizing microscope. The Lumic HC1-LM hot cathode CL microscope operated at 14 kV, 0.0001 mbar and ~0.6 mA electron beam and 2.5 A filament current, respectively.

Microstructural analyses are mostly based on qualitative observations, but some quantitative information was obtained by image analysis using the open source software FIJI / ImageJ (Schindelin et al., 2012; Schneider et al., 2012).

175 ## 3.3 Mineralogical and geochemical investigations

18 bulk rock powder samples for mineralogical and geochemical analyses were prepared with a jaw crusher, subsequent sieving to grain sizes < 62 µm and a McCrone micronization mill providing the < 10 µm grain size fraction.

3.3.1 X-ray diffraction analysis

The mineralogical compositions of the samples were determined by X-ray diffraction (XRD) analysis on random powder
180 samples loaded from the back-side of the sample holders (∅ 16 mm). XRD analyses were performed with a PANalytical Empyrean X-ray diffractometer operating with Bragg-Brentano geometry at 40 mA and 40 kV with CuKα radiation and a PIXel 3d detector at a step size of 0.013 °2Θ from 4.6 to 85 °2Θ and 60 s per step.

Mineralogy was determined qualitatively with the EVA software (version 11.0.0.3) by Bruker. Rietveld refinement for quantitative mineralogy was performed using the program BGMN and the graphical user interface Profex (version 3.10.2, Döbelin and Kleeberg, 2015) calibrated for the used diffractometer. The error of quantitative analyses is expected to be in the range of 3 wt%. Goodness of fit was assessed by visually inspecting the differences between measured and modelled diffractograms and by aiming to obtain R_{wp}-values lower than 3, a value arbitrarily chosen (Toby, 2006).

Bulk powder subsamples (45 mg), dispersed in 1.5 ml of de-ionized water and disaggregated in an ultrasonic bath, were placed on round ($\varnothing$ 3.1 cm) glass slides and air-dried for subsequent smectite and chlorite analyses. Identification of smectite was performed after ethylene glycolation at 45 °C for at least 12 h (2.4 – 25 °2Θ), and heating to 500 °C for one hour allowed to differentiate between chlorite and kaolinite (2.4 – 25 °2Θ, Moore and Reynolds, 1997).

Illite polytype analyses to differentiate between authigenic and detrital (i.e. comminuted muscovite) species were conducted on selected samples with high illte and / or muscovite concentrations (Moore and Reynolds, 1997; Haines and van der Pluijm, 2008). Diffractograms for polytype analyses were acquired between 16 and 44 °2Θ at a step size of 0.013 °2Θ with 200 s per step. All diffractograms and R_{wp}-values are provided in the supplementary material.

3.3.2   X-ray fluorescence spectrometry

X-ray fluorescence spectrometry (XRF) with a PANalytical AXIOS Advanced spectrometer enabled to study geochemical variations of major elements. For this purpose, after drying of ~1.1 g of bulk rock powder overnight at 105 °C, 1 g of sample material, 6 g of $LiBO_2$ and 0.5-0.7 g of ammonium nitrate, acting as oxidizing agent, were fusion digested at increasing temperatures from 400 °C to 1150 °C with a dilution of 1:6. The loss on ignition (LOI) providing volatile contents was determined on 20-30 mg of powder samples with an Euro EA Elemental Analyzer.

To evaluate fluid-related element mobilization, XRF data were analyzed based on the equation of Gresens (1967) for composition-volume relationships resulting from metasomatic alterations, employing the isocon method (Grant, 1986, 2005). In this, the chemical composition of each investigated fault rock sample (i.e. altered rock) is plotted against the chemical composition of the host rock (i.e. unaltered rock). An isocon, a straight line through the origin, separates species enriched relative to the host rock plotting above from those depleted plotting below. It follows the equation

$$C_A = m \times C_H \tag{1}$$

with C_A and C_H being element concentrations of the altered and the host rock, respectively, and m referring to the isocon's slope. A linear best-fit through all data points is used to determine the slope (Grant, 1986, 2005). Enrichment or depletion (ΔC_i) of an element i relative to its host rock equivalent is calculated as follows:

$$\frac{\Delta C_i}{C_i^H} = m \times \frac{C_i^A}{C_i^H} - 1 \tag{2}$$

The inverse of the isocon's slope (m^{-1}) indicates overall mass gain ($m^{-1} > 1$) or loss ($m^{-1} < 1$), respectively. Mass gains [%] are calculated as ($m^{-1} - 1$) × 100 %. A negative mass gain corresponds to a mass loss [%].

Identification of the host rock is just as important as correctly determining the slope of the isocon (Grant, 1986). We defined

215 a reference protolith composition for fault rocks from Havelock Creek, Waikukupa Thrust, Gaunt Creek and DFDP-1A as the average of geochemical compositions of Alpine Schist samples derived from DFDP-2B cuttings (Table S1, Table 4 in Toy et al., 2017).

To assess fluid-related alteration at Martyr River, the geochemistry presented in Table 1 by Spandler et al. (2005) has been averaged to be used as host rock composition (Table S1). However, data from Bluff Complex and Takitimu Mountains have

220 been excluded, because the origin and some geochemical features, respectively, are different from the bulk BST (Spandler et al., 2005). We also note there are limitations to the ability of the isocon-method to understand fluid-assisted alteration related to fault activity at Martyr River. This is because the width of the Alpine Fault deformation zone at this location is larger than the thickness of the BST (Fig. 2b), so faulting-related fluid-rock-interaction with the DMOB likely occurred and the geochemical composition of the reference protolith was already affected by fluid-related alteration. Furthermore, the BST is compositionally

225 very heterogeneous due to magmatic differentiation so it is difficult to choose a single representative geochemical composition of the host rock. Fortunately, these variations only substantially affect the absolute quantification. The method nevertheless allows relative geochemical changes within the fault zone at this location to be accounted for.

The limitations regarding absolute quantification of concentration changes as result of hydrothermal alteration apply to the Alpine Schist, too.

230 ## 4 Results

4.1 Field observations

Individual fault rock units - (ultra)mylonites, cataclasites and footwall gravels - can be identified clearly at all sites investigated. However, weathering and landslides obscure the unambiguous identification of the PSZ, ~~hence the fault core,~~ at Gaunt Creek and Havelock Creek. This is exemplified by an approximately 1 cm thick, fine-grained, brown, fractured and discontinuous

235 layer interpreted to represent the PSZ at Gaunt Creek (Figs. 3c-e) that was identified through sampling to be a footwall-feature approximately 8 cm below the PSZ (see section 4.2.3). Due to these difficult outcrop conditions, measurements of fault orientation are only robust in the well-exposed outcrops at Waikukupa Thrust (50° / 44° SE) and Martyr River (59° / 51° SE) and have to treated with caution at Gaunt Creek (61° / 32° SE) and Havelock Creek (102° / 55° SE).

Thicknesses of fault gouges constituting the PSZ varies between individual locations, including the DFDP-1A core (Figs.

240 3-5), and decreases in the following order: Havelock Creek (~50 cm; Figs. 4a & 5a), Gaunt Creek (~30-40 cm; Figs. 3c-e & 5b), DFDP-1A (20 cm; Fig. 3b), Waikukupa Thrust (~4 cm; Figs. 4b & 5c) and Martyr River (~1-2 cm; Figs. 4c, d & 5d). These thickness variations appear to be not systematically controlled by protolith lithology (Fig. 2; see section 4.3) and highlight that the fault has a very variable character at different locations.
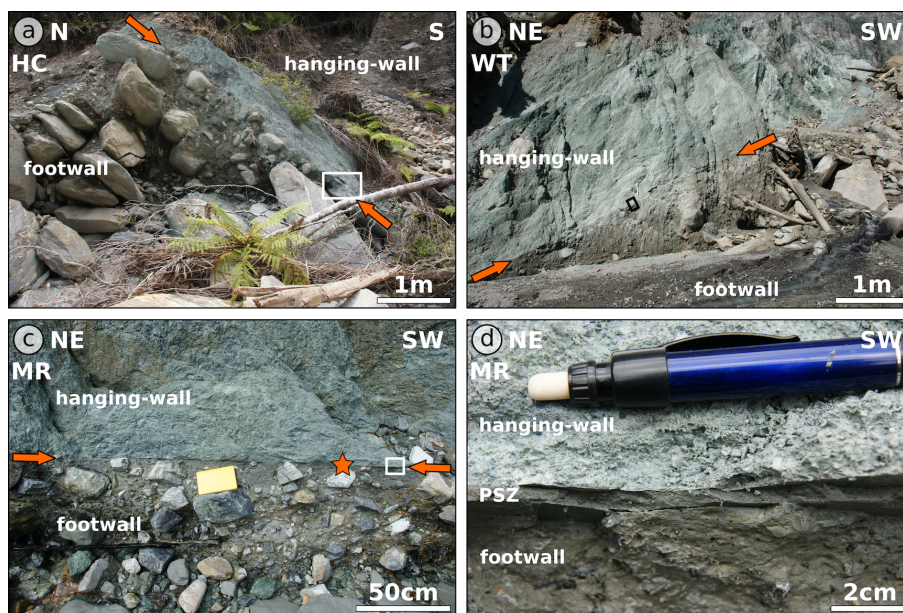
Figure 4. Outcrops of Alpine Fault zone rocks. **(a)** Whereas pale-green hanging-wall cataclasites and larger Quaternary footwall gravels are clearly identified at Havelock Creek, the contacts and hence thickness of the PSZ (indicated by arrows) to over- and underlying units, respectively, are only poorly constrained. White box indicates position of figure 5a. **(b)** The PSZ at Waikukupa Thrust as indicated by arrows is well-defined and straight. Black box gives location of sample presented in figure 5c. **(c)** At Martyr River, hanging- and footwall rocks are sharply separated by a well-defined PSZ (indicated by arrows). White box indicates position of (d). Star gives sample location for specimen shown in figure 5d. **(d)** The PSZ at Martyr River is between 1 and 2 cm thick. HC: Havelock Creek; WT: Waikukupa Thrust; MR: Martyr River.

4.2 Microstructures

245 The fault rocks of Alpine Fault hanging-wall, PSZ and footwall contain clasts embedded in a fine-grained matrix. We define matrix as ~~very~~ fine particles - detrital and authigenic - belonging to the clay-size fraction, i.e. < 2 μm (Fig. 6a). ~~In fact, the typical matrix grain size is~~ ≪ ~~1 μm.~~ The matrix is composed of abundant, predominantly authigenic phyllosilicates - mostly chlorite - and detrital particles, mainly quartz and feldspar. The detrital particles are of subangular to rounded shape with elongate to moderate sphericity and commonly with edges that have been affected by dissolution and mineral alteration processes (Fig.

250 6a).

In contrast, the clasts that are embedded in the fault rock matrix are predominantly comminuted quartz, feldspar and mica grains, as well as fragments of Alpine Schist and mylonite. In addition, there are two more groups of clasts. The first one comprises compact, almost pore-free, fine particles with distinct boundaries but similar composition compared to the surrounding matrix (Fig. 6b). This group of clasts is termed *matrix clasts* in the following. The second group comprises small areas, which

255 are microstructurally similar to *matrix clasts*. These features are characterized by brighter grey-values in BSE-mode, and typi-
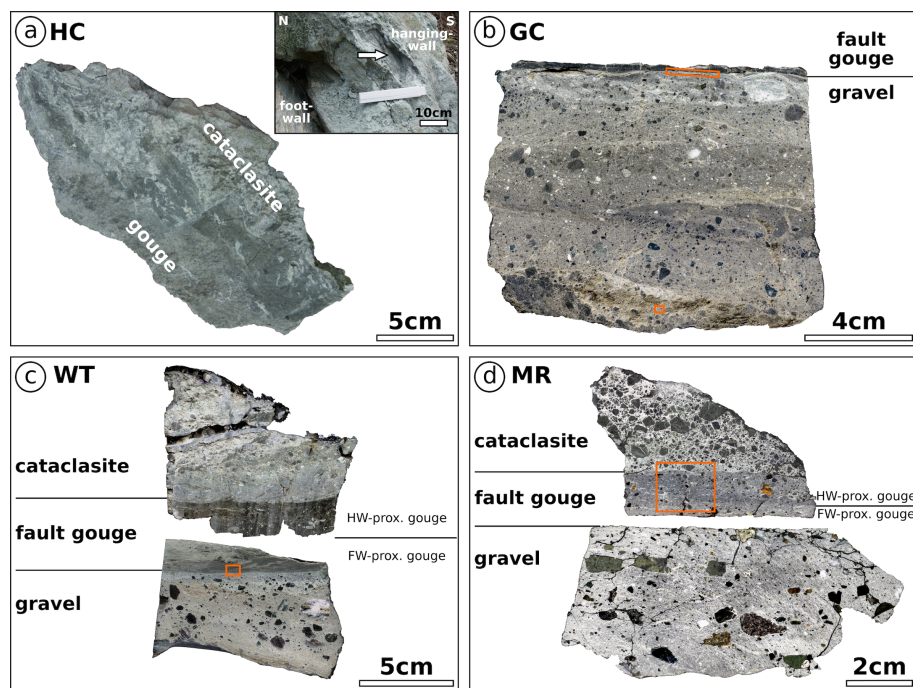
Figure 5. Investigated outcrop samples. **(a)** The contact between hanging-wall cataclasites and thick fault gouge at Havelock Creek is poorly developed and appears to be transitional over ~8 cm. Inset provides zoom to sample location (indicated by arrow). **(b)** Identifying the fault gouge in field at location Gaunt Creek turned out to be difficult. Consequently, only the lowermost part of the PSZ has been sampled. Contact between PSZ and footwall is sharp. Orange box at the contact indicates location of figures 7k-m; orange box at the bottom indicates location of figure 6d. **(c)** The thin fault gouge at Waikukupa Thrust consists of a hanging-wall-proximal and footwall-proximal layer. Orange box gives location of figure 7j. **(d)** The contacts of the thin PSZ with hanging- and footwall rocks, respectively, are sharp at Martyr River. Fault gouge consists of a hanging-wall-proximal and a footwall-proximal layer. Orange box gives location of figures 7a & b. HC: Havelock Creek; GC: Gaunt Creek; WT: Waikukupa Thrust; MR: Martyr River.

cally high porosities allowing to distinguish them from the surrounding material (Fig. 6c). EDX analyses demonstrate that they are compositionally identical to the surrounding matrix. As a comparison of optical and scanning electron microscopy reveals that these structures appear to be similar to *matrix clasts* under plain polarized light (Figs. 6d & e), they will be termed *bright matrix clasts* in the following.

260 ~~The distinct lithological and (micro-to-macro) structural characteristics of all units are described in detail in the following sections and summarized in Tables 1 (hanging-wall), 2 (PSZ) and 3 (footwall).~~

4.2.1 Hanging-wall cataclasites

Clasts embedded in the fine-grained cataclasite matrix at DFDP-1A and Waikukupa Thrust are mostly quartz and feldspars with often fractured, dissolved and altered edges (Fig. 6a). Furthermore, matrix clasts are encountered within close distance
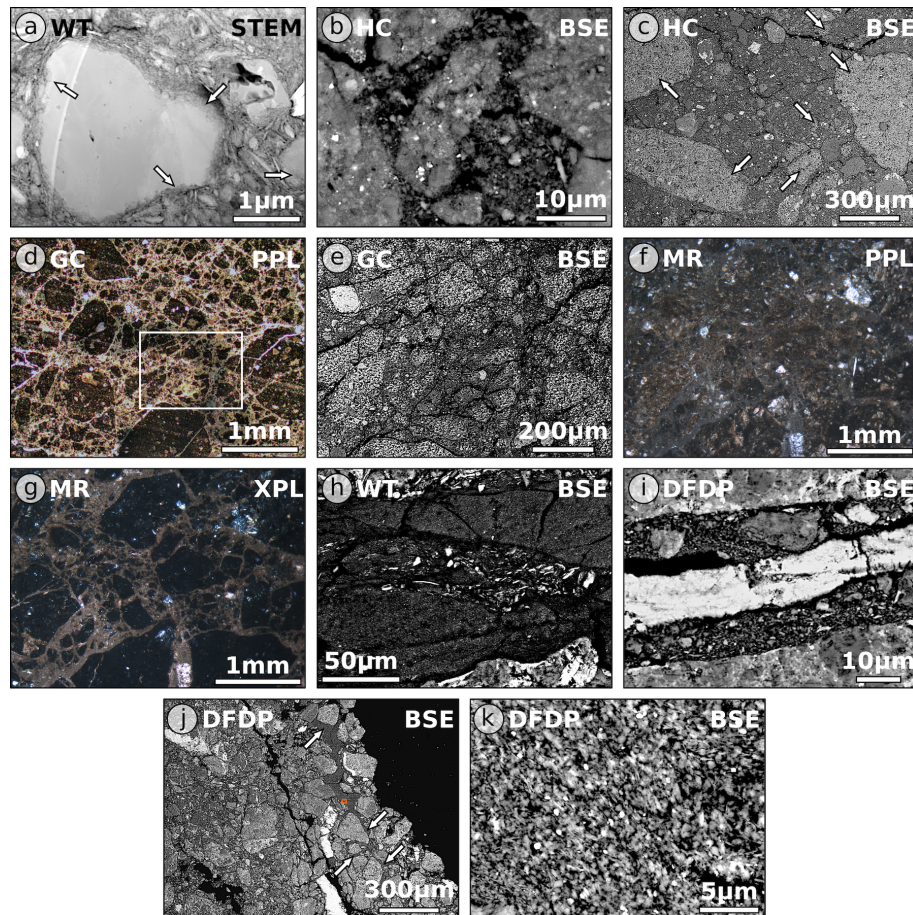
Figure 6. (a) Particles forming the fault rock matrix are defined to be smaller than 2 μm. Abundant authigenic phyllosilicates cement the matrix. Arrows indicate albite dissolution and alteration to phyllosilicates. **(b)** Matrix clasts, low-porosity, compact and clast-like areas of similar composition as the matrix, are embedded within the fault rock matrix at all outcrops. **(c)** Bright matrix clasts (arrows) surrounded by fine-grained matrix and some clasts. **(d)** Lens of matrix clasts within footwall gravels at Gaunt Creek (see figure 5b). White box indicates location of (e). **(e)** SEM analysis shows that clasts within lens ~8-8.5 cm below the PSZ at Gaunt Creek are bright matrix clasts. **(f & g)** Corresponding PPL (f) and XPL (g) photomicrographs of hanging-wall clasts at Martyr River. Identification of constituting mineral phases – mostly quartz, feldspar, chlorite – is only possible by EDX analysis. **(h)** Mature microfault filled by fine-grained authigenic phyllosilicates with typical grain sizes < 2 μm and a core of coarser-grained material. **(i)** Microfault displaying a calcite vein within its core surrounded by fine-grained matrix and some larger clasts. **(j)** Locally, pores and cracks are cemented by fine-grained, authigenic phyllosilicates (arrows). Orange box indicates location of (k). **(k)** Matrix-cementing authigenic phyllosilicates are mostly flake- to needle-shaped chlorite crystallites. WT: Waikukupa Thrust; HC: Havelock Creek; GC: Gaunt Creek; MR: Martyr River; DFDP: Deep Fault Drilling Project core 1A; STEM: scanning transmission electron microscopy; BSE: backscatter electron microscopy; PPL: plane polarized light; XPL: cross-polarized light.

265 to the contact with the PSZ (< 1.35 m at DFDP-1A and < 10 cm at Waikukupa Thrust, respectively). In contrast, quartz and feldspars only constitute ~5 % of clasts at Martyr River. There, most clasts, ~~green on outcrop- and hand specimen-scale (Fig. 5d) but dark-brown to black on the optical microscale (Figs. 6f & g)~~, are identified to be polymineralic aggregates consisting of quartz, feldspar, chlorite, rarely biotite and fragments of calcite veins by EDX analyses. At all locations, there are subordinately fragments of Alpine Schist and mylonites (only Waikukupa Thrust). At DFDP-1A and Waikukupa Thrust they display ~150

270 µm wide, gouge-filled microfaults (Table 1). At Waikukupa Thrust, there are also clay-clast aggregates (CCA; Boutareaud et al., 2008). Amount and size of clasts generally decrease towards the PSZ and vary systematically with PSZ thickness (Table 1): locations with thinner PSZ contain more clasts in the hanging-wall, which tend to be larger, compared to locations with thicker PSZ.

Open cracks, typically several millimeters long and up to hundreds of micrometer wide, increase in abundance towards the

275 PSZ at DFDP-1A and Waikukupa Thrust. Furthermore, microfaults (~5-130 µm wide) cross-cut cataclasites at these locations. They contain comminuted particles and authigenic phyllosilicates and range in maturity: whereas mature microfaults display a well-developed fine-grained fault gouge with particles up to tens of micrometer in size but mostly smaller than 2 µm (Fig. 6h), juvenile microfaults contain poorly sorted particles up to a few hundreds of micrometer in size with the majority being larger than 10 µm. In addition, some microfaults have cores made of coarser-grained matrix and clasts (Fig. 6h) or calcite veins (Fig.

280 6i) surrounded by fine-grained gouge.

Locally, there are patches almost completely devoid of clastic particles but with abundant authigenic flake- to needle-shaped chlorite crystals cementing pores and fractures at Waikukupa Thrust and DFDP-1A (Figs. 6j & k). The amount of these chlorite-dominated areas as well as authigenic phyllosilicates in general increases with decreasing distance to the PSZ and progressively cements the fault rocks. Furthermore, the matrix is cemented by calcite (Table 1). Whereas finely-dispersed calcite is abundant

285 at Martyr River, calcite at Waikukupa Thrust is mostly present only in direct vicinity (< 3 cm) to the PSZ. There, mutually cross-cutting calcite veins (~15 µm thick) display small (< 20 µm) dextral offsets. Furthermore, there are < 100 µm large calcite-cemented breccias composed of angular fragments of clastic particles and *matrix clasts* (see figure 3c in Schuck et al., 2018). At DFDP-1A, calcite is encountered in lenses and veins, which frequently cross-cut clasts but rarely the matrix and generally increase in abundance towards the PSZ.

290 Locally, cataclasites are foliated. At DFDP-1A, clasts together with microfaults define a weak foliation varying non-systematically across the investigated interval, locally displaying SC-geometry. At Waikukupa Thrust and close to the PSZ, cataclastic lenses exhibit a very weak foliation parallel to displacement.

4.2.2 Principal Slip Zone fault gouges

The type of contact between hanging-wall cataclasites and fault gouge correlates with PSZ thickness: where the PSZ is thicker,

295 contacts are transitional manifested by decreasing grain sizes (Table 2) and correlate with increasing amounts of phyllosilicates, as exemplified at Havelock Creek with its transitional, poorly-developed contact over 8 cm (Fig. 5a). In contrast, Waikukupa Thrust has a sharp contact on the outcrop and hand-specimen scale (Figs. 4b & 5c), but displays a transition over 4 mm from a porous, clast-rich cataclasite-matrix to a very dense PSZ-matrix as revealed by microscopic inspection (see figure 3a in Schuck
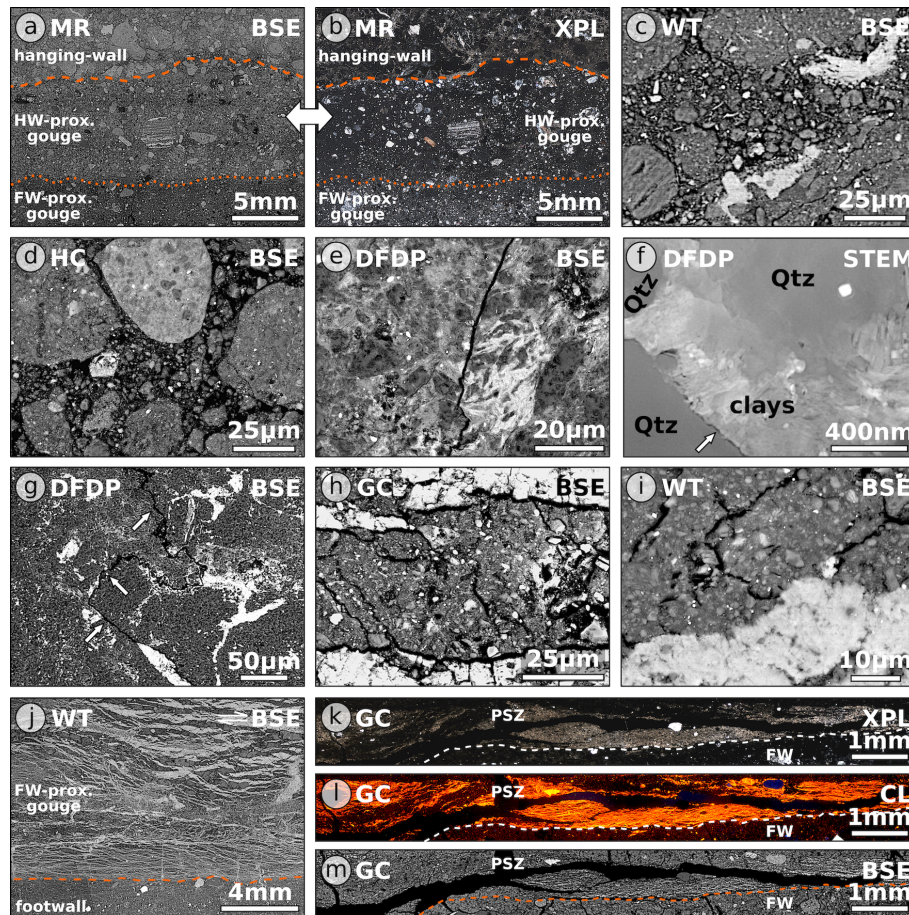
Figure 7. (a & b) Corresponding BSE (a) and XPL (b) photomicrographs of the fault core at Martyr River. Identification of the contact between hanging-wall and PSZ (stippled line) as well as hanging-wall and footwall-proximal gouge (dotted line), respectively, is difficult. **(c & d)** The hanging-wall proximal gouge at Waikukupa Thrust (c) with its large amount of matrix clasts is microstructurally similar to the PSZ at Havelock Creek (d). **(e)** Photomicrograph of typical microstructures of cemented PSZ at DFDP-1A core. **(f)** Cemented PSZ matrix of the DFDP-1A core. Pores between comminuted and dissolved (arrow) quartz grains are cemented by authigenic phyllosilicates, mainly chlorite. **(g)** Slickolite (white arrows) indicative of pressure solution. **(h & i)** Fault gouge at Gaunt Creek (h) is microstructurally similar to footwall-proximal gouge at Waikukupa Thrust (i). **(j)** Network of anastomosing calcite veins within footwall-proximal gouge layer at Waikukupa Thrust. The contact between fault gouge and footwall (orange line) is sharp. **(k-m)** The basal part of the PSZ at Gaunt Creek hosts a network of calcite veins terminating at the sharp contact (white / orange stippled line) with the footwall (FW). MR: Martyr River; WT: Waikukupa Thrust; HC: Havelock Creek; DFDP: Deep Fault Drilling Project conA; GC: Gaunt Creek; BSE: backscatter electron microscopy; XPL: cross-polarized light; STEM: scanning transmission electron microscopy; CL: cathodoluminescence.

et al., 2018). Identification of the sharp but undulating contact at Martyr River is simple on outcrop- and hand-specimen (Figs. 4c, d & 5d), but difficult on microscale (Figs. 7a & b).

Matrix clasts are the prevailing type of clast at Waikukupa Thrust and Havelock Creek (Figs. 7c & d), but constitute less than 5 % of clasts at Martyr River. Furthermore, unlike Martyr River, where large, fine-grained chloritized particles dominate in the hanging-wall, the calcite-poor, phyllosilicate-cemented fault gouge at this location hosts individual mineral phases (Fig. 7b). *Bright matrix clasts* are present at all locations, but are abundant only at Havelock Creek and Gaunt Creek, where they, in

305   addition to clast-like shapes, occupy several hundreds of micrometer large areas. In general, amount and size of clasts weakly correlates with PSZ thickness (Table 2). Where the PSZ is thinner, clasts tend to be more abundant and sizes tend to be larger. Clast sizes increase in the following order: Gaunt Creek (~75 μm), Havelock Creek (~75 μm), Waikukupa Thrust (~100 μm) and Martyr River (tens of micrometer to ~200 μm).

It is not possible to determine the amount and size of clasts within the DFDP-1A core, because more than 90 % of this

310   unit is cemented by authigenic phyllosilicates, mostly chlorite (Figs. 7e & f). Authigenic phyllosilicates tend to nucleate along crack and grain boundaries of fractured grains. Additionally, newly formed phyllosilicates replace dissolved larger particles and mimic their original shape. Non-cemented areas are restricted to fractures. Many of these fractures contain up to 350 μm wide calcite ~~cores~~, locally surrounded by gouge, microstructurally similar to microfaults observed within the DFDP-1A cataclasites (see Fig. 6i). It is at these non-cemented, fracture-related locations that there are patches of fine-grained, randomly oriented

315   and needle-shaped, authigenic chlorite crystallites. The presence of these patches within the PSZ is restricted to DFDP-1A.

DFDP-1A is the only location investigated, where there are indications of deformation by pressure-solution as evidenced by a ~~slickolite (Fig. 7g), a~~ stylolite with teeth oblique to the stylolite surface (cf. Passchier and Trouw, 2005). ~~However, enrichment of insoluble material or secondary phases along teeth-crowns is not observed.~~

PSZs at Waikukupa Thrust and Martyr River are layered and display a hanging-wall-proximal and a footwall-proximal layer,

320   respectively (Figs. 5c & d). At Martyr River, the contact is best recognized on the hand-specimen scale (Figs. 4d, 5d, 7a & b), where the fault gouge is blueish-grey proximal to the hanging-wall and green-grey proximal to the footwall. Minor differences between both gouge layers are manifested by slightly more and larger clasts in the ~0.8-1 cm thick hanging-wall-proximal layer than the ~0.3-0.5 cm thick footwall-proximal layer (20-25 % vs. 25-30 %; Table 2).

At Waikukupa Thrust, a sharp but undulating contact separates a brown-dark grey hanging-wall-proximal layer with 5-10 %

325   clasts from a medium-light grey footwall-proximal layer, which is clast-poor (< 1 % clasts; usually < 5 μm large).

The dense, clast-poor (< 1 % clasts) fault gouge at Gaunt Creek is microstructurally identical to the footwall-proximal layer at Waikukupa Thrust (Figs. 7h & i). Furthermore, both gouges exhibit calcite vein networks close to the contact with the footwall (Figs. 7j-m). At Waikukupa Thrust, veins display mutual cross-cutting relationships with dextral offsets. For a detailed description of these calcite veins, the reader is referred to the preceding work of Schuck et al. (2018). At Gaunt Creek,

330   the 350-800 μm wide vein network (Figs. 7k-m) is subject to intensive fracturing and calcite dissolution, which hampers the identification of cross-cutting relationships. Furthermore, the contact between calcite veins and surrounding gouge is poorly-developed. Veins are typically 5-10 μm wide and tend to be thicker, less dissolved and deformed close to the footwall. CL colors are yellow-orange but slightly brighter and more yellow towards the footwall (Fig. 7l).

Apart from these vein networks, calcite veins cross-cut *matrix clasts* at Martyr River and the hanging-wall-proximal gouge

335   layer of Waikukupa Thrust, but are very rare at Havelock Creek. Additional hanging-wall-proximal microstructures are clasts

forming a weak foliation parallel to displacement at Martyr River and CCAs at Waikukupa Thrust. Furthermore, hanging-wall proximal microstructures at Waikukupa Thrust are similar to those of Havelock Creek (Figs. 7c & d), except that clasts are not homogenously distributed but cluster randomly at Havelock Creek. Apart from the hanging-wall-proximal fault gouge layer of Waikukupa Thrust, where typical clast size decreases while the size of *matrix clasts* increases towards the footwall, trends
340 regarding microstructures are not observed. Most remarkably, there are no discrete slip planes within the fault gouges.

4.2.3 Footwall gravels

The contact between clast-poor PSZ and clast-bearing footwall is sharp (Figs. 4b-d; 5b & c; 7j–m). Footwall gravels are compositionally similar to overlying hanging-wall cataclasites and fault gouges (Table 3). Furthermore, correlations regarding amount and size of clasts as observed in hanging-wall cataclasites and fault gouges are valid within footwall gravels, too
345 (Table 3): locations with thin PSZ tend to contain more and larger clasts than locations with thicker PSZ. In addition, grain size increases with increasing distance from the PSZ. Whereas there are some bright *matrix clasts* at Martyr River and Gaunt Creek, *matrix clasts* are only encountered at Gaunt Creek. At Martyr River, footwall clasts are slightly imbricated and have a weak foliation parallel to displacement.

Calcite is absent at Martyr River and restricted to a ~3 mm thick layer immediately adjacent to the PSZ at Waikukupa Thrust.
350 There, calcite constitutes finely dispersed cement, veinlets and < 5 μm thick rims at grain edges parallel to displacement. In contrast, at Gaunt Creek, calcite is predominantly found in veins and lenses cross-cutting matrix and detrital clasts.

The ~1 cm thick, fine-grained, brown layer erroneously interpreted as PSZ at Gaunt Creek (Figs. 3d & e), is mainly composed of fractured, subangular to subrounded *matrix clasts* (Fig. 6d). The amount of quartzofeldspathic clasts within this lens is < 5 %. Fractures between the individual clasts are filled with a fine-grained matrix. SEM analysis reveals that these clasts are
355 actually *bright matrix clasts* (Fig. 6e).

4.3 Mineralogy

There are only minor variations in qualitative fault rock composition (Table 4). Quartz, feldspar, calcite and phyllosilicates, (chlorite, kaolinite, muscovite, illite, and biotite) and traces of apatite, pyrite and rutile are always present. Additionally, Waikukupa Thrust and Havelock Creek contain amphiboles, mainly hornblende, and there is epidote at Waikukupa Thrust and Martyr River. Serpentine minerals are only encountered within the fault gouge at Martyr River. Analyzed fault rocks do
360 not contain smectite, and kaolinite is present only in traces. Furthermore, polytype analysis demonstrates that illite identified by Rietveld refinement predominantly constitutes detrital but comminuted muscovite (see supplement).

4.3.1 Hanging-wall cataclasites

Quartz and feldspars are the dominant mineral phases in hanging-wall cataclasites. They do not exhibit any clear trend towards
365 the PSZ (Table 4). Phyllosilicates appear to decrease in content towards the PSZ. This probably is an artefact of Rietveld refinement based on the < 10 μm instead of the clay-size fraction. In the DFDP-1A drill core material, the concentrations

Solid Earth
Discussions
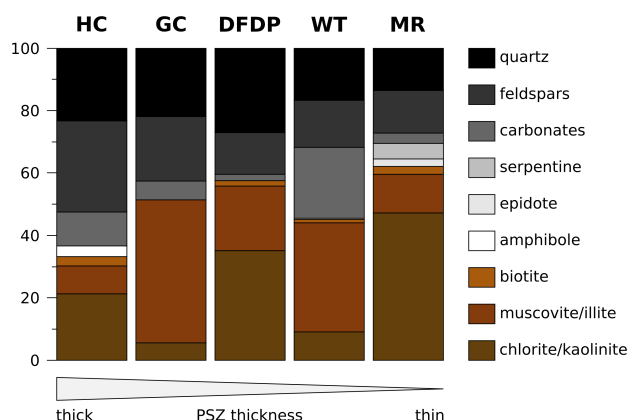
Figure 8. Simplified mineralogical composition of investigated PSZs based on results presented in Table 4. HC: Havelock Creek; GC: Gaunt Creek; DFDP: Deep Fault Drilling Project core 1A.; WT: Waikukupa Thrust; MR: Martyr River.

of detrital muscovite/illite decrease towards the PSZ compared to authigenic chlorite/kaolinite showing an opposite trend. Furthermore, calcite also increases towards the PSZ at DFDP-1A.

4.3.2 Principal Slip Zone fault gouges

370   Quartz and feldspar contents vary by more than 50 % between individual locations (21 wt% at Waikukupa Thrust vs. 52 wt% at Havelock Creek; Table 4). In general, these clastic phases tend to be less abundant in thinner than in thicker PSZs (Fig. 8). Phyllosilicate concentrations exhibit the opposite pattern: thinner PSZs tend to be more phyllosilicate-rich than ticker PSZs. Furthermore, chlorite/kaolinite and muscovite/illte show inverse correlations but do not vary systematically with respect to PSZ thickness. Calcite concentrations of Waikukupa Thrust (29 %) and Gaunt Creek (6 %) reflect mineralization manifested

375   in vein networks. As calcite veins are rare at Havelock Creek, the relatively high (11 %) concentrations potentially reflect calcite cementation. In contrast, calcite concentrations within PSZs of DFDP-1A and Martyr River are lower compared to the hanging-wall.

4.4 Geochemistry

Element concentrations commonly scatter and, if at all, increase or decrease only slightly towards the PSZs (Table 5). The

380   isocon analysis reveals a slight but recognizable correlation between the amount of fluid-related alteration and PSZ thickness; using the slope of the isocon as a proxy to assess the overall degree of fluid-related alteration, with a larger deviation from one indicating a higher amount of alteration, the hanging- and footwalls of sample locations with thinner PSZ are generally less affected by metasomatism (Fig. 9; Table 6; Tables S1 & S2). The PSZs display the same trend, but less pronounced. This is especially valid for the PSZ at Waikukupa Thrust, which is affected by a fluid-related mass change of up to 79 %. However,
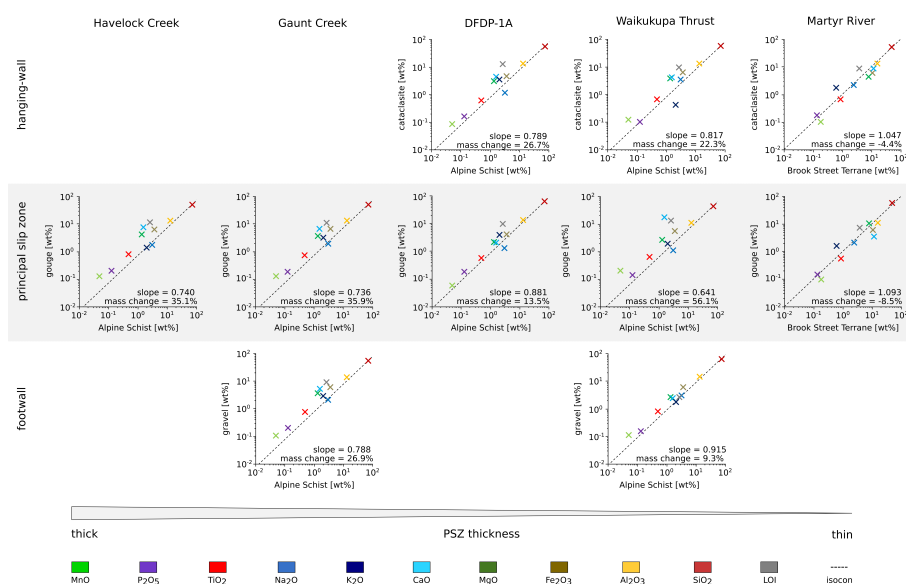
Figure 9. Isocon analysis of locations investigated. In case of multiple measurements per structural unit (hanging-wall, PSZ, footwall), data were averaged to derive single values. Values are given in Table S1.

microstructural observations (see section 4.2.2 and Schuck et al., 2018) indicate this is most likely related to the extraordinarilly large amount of calcite veins.

Enrichment of individual elements confirms this correlation: enrichment of Al_2O_3, CaO and LOI in hanging- and footwall rocks is more pronounced at locations with thicker PSZ compared to those with thinner PSZ (Table 6; Table S2). Element enrichment of PSZ fault gouges exhibits a similar but less pronounced trend with CaO at Waikukupa Thrust being remarkably more enriched than expected due to formation of calcite veins.

Looking at cross-fault transects, the degree of metasomatism at DFDP-1A increases towards the PSZ and displays highest hanging-wall amounts immediately adjacent to the PSZ (Table 6). Furthermore, whereas the PSZ at DFDP-1A has been less affected by fluid-related alteration compared to the hanging-wall, samples of Waikukupa Thrust display a continuing trend to higher amounts of fluid-related alteration from the hanging-wall to the base of the PSZ close to the footwall.

Footwalls are generally less affected by metasomatism than hanging-walls and PSZs. Despite limited sample numbers, the degree of metasomatism at Gaunt Creek appears to decrease with increasing distance to the PSZ.

5   Discussion

5.1   Fluid-related alteration and fluid transport within Alpine Fault rocks

Isocon analyses clearly demonstrate that all investigated fault rocks have been substantially altered by fluids (Fig. 9; Table 6), which is also shown by the presence of calcite vein networks and authigenic phyllosilicates. In general, metasomatic alteration

of the fault rocks resulted in element enrichment and mass gain. Analyses of Martyr River fault rocks seem to show an opposite pattern but this may be an artefact related to inappropriate choice of the protolith's geochemical composition (see section 3.3.1).

While the degree of fluid-related alteration correlates slightly with fault gouge thickness (Fig. 9; Table 6), it is correlated negatively with phyllosilicate content (Figs. 8 & 9). Furthermore, except for the ~~slickolite~~ observed in the DFDP-1A fault core

405 (Fig. 7g), there is no microstructural evidence for pressure-solution such as dissolution seams or indented and embayed clasts. Considering the large amounts of annual rainfall along the NW edge of the Southern Alps, it is likely the observed dissolution of grain edges is related to weathering rather than fault deformation processes.

In summary, both microstructures and the predominant enrichment of elements show that fluids are not responsible for stress-driven dissolution processes or for substantial mass transfer out of the fault zone. Except for Ca-enrichment due to formation

410 of calcite networks at Gaunt Creek and Waikukupa Thrust, the results of this study do not identify alteration mechanisms that completely explain the observed element mobilization within the fault rocks.

It is recognized that the Alpine Fault's PSZ constitutes an impermeable barrier restricting fluid circulation to its hanging-wall (Sutherland et al., 2012; Menzies et al., 2016). Consequently, fluid-related element mobilization can be expected in the hanging-wall. This is confirmed by isocon analyses: DFDP-1A samples show increasing degrees of fluid-related alteration

415 towards the PSZ with peak-values immediately above it. However, all other locations display fault gouges more affected by fluid-related alteration than hanging- and footwall rocks, respectively. In combination with networks of anastomosing calcite veins (Figs. 7j-m; Schuck et al., 2018), this suggests that there is repeated transient fluid-flow within the PSZ, most-likely along-fault as indicated by veins oriented parallel to displacement.

Results of isocon analyses also confirm outcomes of previous studies, which demonstrated that fluid-related alteration sig-

420 nificantly changed the petrophysical, mineralogical, geochemical and geomechanical properties of the Alpine Fault zone (e.g. Boulton et al., 2012; Townend et al., 2013; Carpenter et al., 2014). This supports the proposal of Sutherland et al. (2012) that an 'alteration zone' within ~50 m of the PSZ should be included as a fundamental and additional part of the Alpine Fault zone architectural model (Fig. 2c).

5.2 Architecture of Alpine Fault zone

425 5.2.1 Alpine Fault damage zone

Norris and Cooper (2007) suggested an average brittle damage zone width based on a compilation of outcrop studies in the fault's central segment ~~of ~100 m~~. More recent investigations indicate wider damage zones: Alpine Fault outcrops in the segment south of Haast have damage zone widths between 90 and 240 m (Barth et al., 2013). Analyses of downhole geophysical data and recovered cores from the DFDP-2 borehole indicate that the Alpine Fault's hydrologically active damage

430 zone, where fluids circulate in fractures ~~that are more common than in the surrounding rock mass~~, contains an 'inner zone' affected by earthquake rupture processes that is 0.5 km wide at up to 8 km depth and about 1 km wide at the surface (Fig. 2c). This inner damage zone is surrounded by an up to a few kilometers wide 'outer zone', which might be a near-surface, topographically-controlled feature only (Townend et al., 2017; Massiot et al., 2018; Williams et al., 2018).

Outcrop and drillcore investigations demonstrate quite constant fracture densities within at least 500 m of the PSZ in the
hanging-wall and 30 m in the footwall (Williams et al., 2016, 2018), which is different to decreasing fracture densities towards
the fault cores observed elsewhere (e.g. Chester et al., 2005; Faulkner et al., 2006; Mitchel and Faulkner, 2009). In fact, DFDP
investigations show that apparent fracture density decreases with depth, i.e. towards the PSZ (Townend et al., 2013; Williams
et al., 2016). However, this is considered as an artefact resulting from rapid exhumation and associated unloading (Williams
et al., 2016). Furthermore, despite its presence across the entire damage zone, gouge-filled fractures within < 160 m of the PSZ
tend to be thinner (< 1 cm) and more abundant (Williams et al., 2018).

5.2.2 Alpine Fault core

Extent of fault core

As a result of the pervasive alteration zone surrounding the PSZ, the fault core of the Alpine Fault is rather diffuse (Sutherland
et al., 2012; Townend et al., 2013; Williams et al., 2018). Commonly, the fault gouge forming the PSZ and part of the sur-
rounding cataclasites are considered to constitute the fault core (e.g. Williams et al., 2017). However, there is some ambiguity
when it comes to actually defining the width of the fault core: Toy et al. (2015) consider a 20-30 m wide zone around the PSZ
as fault core, Sutherland et al. (2012) and Townend et al. (2017) narrow it down to 2 m surrounding the PSZ with an additional
degree of localization manifested in the < 0.5 m wide PSZ (Sutherland et al., 2012; Williams et al., 2016). However, by defining
the damage zone as having elevated fracture densities compared to the host rock (Chester et al., 1993; Faulkner et al., 2010)
and noting that there is no observable variation in fracture density within 30 m of the PSZ (Williams et al., 2016), it seems
reasonable to exclusively consider the fault gouge forming the PSZ as core of the Alpine Fault's central segment. This view is
supported by fault gouge microstructures; microfaults (Figs. 6h & i), predominantly encountered in hanging-wall cataclasites
but also present in fault gouges (Table 3), show that strain is localized to discrete structures within the PSZ. Furthermore,
these structures exhibit a broad range in degree of sorting (poorly – very well) and grain size (< 2-100s of micrometer), which
demonstrates that they accommodated different amounts of strain. However, microfaults appear to be a local phenomenon and
there are no continuous, discrete slip planes within the PSZ, despite the large finite displacement accommodated.

This interpretation is further backed by distinct geophysical (e.g. Townend et al., 2013), petrophysical (e.g. Carpenter et al.,
2014), mineralogical (e.g. Schleicher et al., 2015), microstructural (e.g. Toy et al., 2015) and geochemical (Schuck et al., 2018)
properties of the PSZ. To the SW of the study area, the fault core might be more complex, because of its different lithological
composition and fault orientation (Barth et al., 2013).

Fault-core along-strike variations

Despite mostly comparable microstructures and mineralogy of investigated fault rocks (Tables 1-4), there are complex along-
strike variations of fault gouge properties. In the following, we relate the results of our microstructural and geochemical
investigation to the geometry of the Alpine Fault zone and its spatial variations. Furthermore, we examine whether the fault
core structures result from shallow-depth phenomena, thus do not provide information about deeper fault zone architecture.
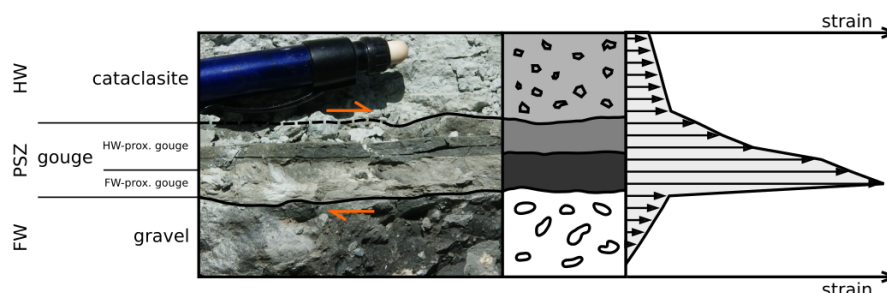
Figure 10. Conceptual model providing a potential explanation how layered principal slip zones observed at Martyr River and Waikukupa Thrust could have been formed. Resulting from the juxtaposition of weakly consolidated sediments in the footwall and relatively competent fault rocks, strain localized non-homogenously in the PSZ. Example is from Waikukupa Thrust. Stippled line indicates where contact between cataclasite and gouge is obscured by debris. Figure was modified according to Cowan et al. (2003).

Fault gouges at Waikukupa Thrust and Martyr River are layered. However, continuous transects across the fault core, which sample contacts of fault gouge with hanging- as well as footwall rocks respectively, and which allow microstructures to be described across the entire PSZ, are only available from these two outcrops. Consequently, the absence of layered fault gouges at other locations seems to be more appropriately explained by a sampling bias than by fault gouge layers being site-specific features.

Cowan et al. (2003) analyzed low-angle detachment faults in the Death Valley, where layered fault gouges separate footwall cataclasites from weakly consolidated hanging-wall sediments. Compared to the footwall-proximal gouge layer, the hanging-wall-proximal layer is fine-grained, clast-poor and supposed to have accommodated most of the strain. Changing boundary conditions during exhumation, namely decreasing temperature and pressure, as well as fluid-related alteration leading to the formation of authigenic phyllosilicates and juxtaposition of fault rocks with hanging-wall sediments resulted in mechanical layering enabling the hanging-wall-proximal layer to accommodate most of the strain.

By considering the different fault kinematics (low-angle detachment vs. thrust fault), the Alpine Fault with its layered gouges described in this and previous work (e.g. Boulton et al., 2012; Schuck et al., 2018) is structurally identical to the faults analyzed in the Death Valley (Fig. 10; for details see Biegel and Sammis, 2004). The footwall-proximal layer of Alpine Fault gouge contains fewer and preferentially smaller clasts than the overlying hanging-wall-proximal layer (Table 2) and bounds mechanically weak gravels. Furthermore, microstructures of the calcite network in the footwall-proximal layer at Waikukupa Thrust attest to localized and cyclic faulting (Schuck et al., 2018) supporting the interpretation that this gouge unit accommodated most of the strain. Consequently, layered fault gouges and associated microstructural evidence demonstrate that strain localization and associated structural complexities within the Alpine Fault core are, at least partially, affected by shallow, hence late, processes.

This interpretation has major consequences for structural investigations of the Alpine Fault's PSZ, because it implies that formation of microstructures observed in outcrops was influenced by boundary conditions not representative of those along

Solid Earth
Discussions
Open Access
EGU

most of the fault rocks' exhumation path. This highlights the importance of continuing to attempt to obtain samples for microstructural investigations of Alpine Fault rocks from locations and / or depths, where hanging-wall and PSZ fault rocks are

490 not juxtaposed on weakly consolidated footwall sediments.

The most remarkable difference between individual locations is variation in PSZ thickness by a factor of of 25 (2 cm at Martyr River vs. 50 cm at Havelock Creek; Figs. 3-5). Furthermore, locations with thicker PSZ tend to have poorly defined contacts with hanging- and footwall respectively, than locations with thinner PSZ (Table 2). It has been suggested that such variations may result from different mechanisms of deformation (Hobbs et al., 1990; Schrank et al., 2008), or initial presence of

495 heterogeneities subsequently amplified during continuous deformation (Segall and Pollard, 1983; Schrank et al., 2008; Norris and Toy, 2014; Fossen and Cavalcante, 2017). Common examples are variations in mechanical strength reflecting differing viscosities as result of compositional heterogeneities (Chester et al., 1993; Faulkner et al., 2003; Schrank et al., 2008; Rybacki et al., 2014; Nardini et al., 2018), varying geometric properties (Cowan et al., 2003; Schrank et al., 2008) or a combination of all or some of these factors (Schrank et al., 2008; Boese et al., 2012; Czaplinska et al., 2015).

500 These explanations do not appear to be responsible for observed variations as there is no correlation between PSZ thickness and sample location along-strike (Fig. 2b). Furthermore, all locations, except Martyr River, are in the central segment of the Alpine Fault where Torlesse Terrane Alpine Schist is the protolith. This demonstrates that variations of protolith mineralogy have no significant influence on observed differences in PSZ thickness. However, fault gouge thickness correlates with mineralogy: thicker gouges at Havelock Creek, Gaunt Creek and the DFDP-1A core are richer in clastic phases and poorer in

505 phyllosilicates than the thin gouges of Martyr River and Waikukupa Thrust (Fig. 8). This is astonishing, because phyllosilicate-rich fault gouges generally tend to be wider (Faulkner et al., 2003; Schleicher et al., 2009) owing the frictionally weak nature of these phases (Moore et al., 1997; Moore and Lockner, 2007; Lockner et al., 2011; Carpenter et al., 2015). Furthermore, the very narrow fault gouge at Martyr River contains frictionally extraordinary weak serpentine phases which elsewhere have typically dominated in fairly thick fault zones (Moore et al., 1997; Moore and Rymer, 2007, 2012). Conversely, fault zones

510 with similar quartzofeldspathic composition to the Alpine Fault are typically narrower (Chester et al., 1993; Faulkner et al., 2003). Consequently, unlike other fault zones worldwide, the Alpine Fault displays a negative correlation between phyllosilicate content and fault core thickness. This suggests that strain localization within the fault core might be governed by processes insensitive of rheological variations caused by differing fault rock composition.

In addition, orientation of the fault (Figs. 2a & b), magnitude of stress and the stress field itself (Boese et al., 2012; Warren-

515 Smith et al., 2017) are fairly constant along the central segment of the Alpine Fault, thus it is unlikely that these parameters are responsible for observed variations of fault gouge thickness. Biegel and Sammis (2004) suggested to explain along-strike variations of gouge thickness as record of rupture arrest. However, our observations (and the nature of Alpine Fault outcrops in general) do not easily lend themselves to a systematic analysis of this kind in the Alpine Fault zone.

Another approach to explain observed thickness variations is to examine the relation between fault core width and displace-

520 ment. Wear models describe a positive correlation between gouge thickness and displacement (e.g. Hull, 1988; Scholz, 1987). However, quantitative models of fault core evolution have so far failed to reproduce datasets compiled on natural faults (e.g. Blenkinsop, 1989; Evans, 1990; Sibson, 2003). Nevertheless, faults that accommodated larger displacements do appear to gen-

erally have thicker fault cores (Evans, 1990; Faulkner et al., 2010; Ben-Zion and Sammis, 2003, and references therein). In other words: the more earthquakes a fault has seen, the thicker its PSZ may be (Ma et al., 2006; Li et al., 2013). However,

525   by keeping in mind that four of the five fault gouges investigated are located in the Alpine Fault's central segment, which is considered to rupture entirely during an earthquake (Sutherland et al., 2007; Howarth et al., 2018), and in absence of other processes considered likely, PSZ thickness variations suggest that studied fault gouges accommodated different amounts of displacement. This implies the studied PSZs are not part of the same shear plane, and that the Alpine Fault zone hosts multiple fault strands, which may not be active simultaneously during the same events (Fig. 1b).

530   This assumption of a more complex Alpine Fault zone geometry is further supported by microstructural, mineralogical and geophysical observations ~~to be discussed in the following~~. Most obviously, the two PSZs encountered in the DFDP-1B core (Fig. 3a; Toy et al., 2015) promote a more complex view of fault zone architecture. Furthermore, although the shallower DFDP-1B PSZ and the PSZ of DFDP-1A have so far been considered to belong to the same fault plane (Fig. 3a), they exhibit different mineralogical and hence geomechanical properties (Boulton et al., 2014; Schleicher et al., 2015). This is unexpected

535   given the small separation between boreholes and thus sample spacing of less than 100 m (Sutherland et al., 2012). Similarly, although mineralogically comparable (Fig. 8), fault gouge microstructures of DFDP-1A and Gaunt Creek, also within only ~100 m distance (Fig. 3a), differ remarkably, as exemplified by the almost completely cemented DFDP-1A PSZ compared to the PSZ at Gaunt Creek (Table 2; Figs. 7e, f, k-m).

In light of this interpretation, the ~1 cm thick, *matrix clast*-bearing layer sampled ~8 cm below the PSZ at Gaunt Creek

540   (Figs. 3d, e, 5b & 6d), which is microstructurally similar to the investigated fault gouges at Havelock Creek and Waikukupa Thrust (hanging-wall-proximal layer), could be considered to constitute another PSZ of the Alpine Fault, currently starting to accommodate larger amounts of slip or an inactive one as observed in the fault's southern segment (Barth et al., 2013).

Consequently, this multidisciplinary approach reveals that the Alpine Fault zone has a complex geometry, which is atypical for quartzofeldspathic faults but typical for carbonate or phyllosilicate-hosted ones. Nonetheless, it cannot be excluded that the

545   observations we present in favor of a more complex fault zone geometry simply reflect shallow-depth phenomena like layered fault gouges do. However, seismic investigations that extend into the basement at the DFDP-2 site and around Haast also support a more complex fault zone model. These studies imaged a series of subparallel reflectors, interpreted as multiple fault strands (Lay et al., 2016; Lukács et al., 2018). So far, it is debated if these separate fault strands are isolated or anastomosing and if they are/were active contemporaneously or consecutively (Lukács et al., 2018). Note that this structural complexity

550   differs from the situation encountered at Waikukupa Thrust, as the second fault strand encountered at Hare Mare Creek, 700 m to the NE of this location, resulted from incision of the Waikukupa River and subsequent stress reorientation (Norris and Cooper, 1997).

6   Conclusions

Rheological contrasts resulting from the juxtaposition of poorly consolidated and mechanically weak footwall sediments with

555   more competent hanging-wall cataclasites control strain localization within the fault gouge and result in a layered structure at

shallow depths. The possibility that topography also influences gouge thickness at shallow depth should be considered based on further work combining field, laboratory and geomorphologic investigations. These results also show that careful analyses are necessary in order to study actively exhumed fault zones as microstructures may rather record shallow-depth artefacts than deformation history.

560   Field and borehole observations supported by microstructural, mineralogical and geochemical analyses provide evidence that the Alpine Fault zone is more complex than suggested by previous field investigations, which were hampered by the dense vegetation of the study area. These results highlight that the fault has a very variable character at different locations, and that this character is demonstrably not systematically controlled by the protolith lithology. Interestingly, PSZ width is not only unaffected by mineralogical composition but also correlates negatively with phyllosilicate content, which is different from

565   other fault zones around the world where phyllosilicate-rich faults tend to be less localized.

     Consequently, these combined microstructural, mineralogical and geochemical analyses, considered in context of other studies, show the Alpine Fault zone architecture is more appropriately described by the broad and complex conceptual model of Faulkner et al. (2003) rather than the simple, single PSZ model of Caine et al. (1996). This suggests that investigated fault gouges are not part of the same fault plane but represent distinct slip planes within a complex network of anastomosing shear

570   planes forming the core of the Alpine Fault, surrounded by a broader damage zone. As other commonly invoked approaches, such as compositional heterogeneities, do not explain observed differences, varying fault gouges thicknesses demonstrate that individual slip planes accommodated different amounts of displacement, hence strain. Dating ~~encountered~~ fault gouges would allow assessment of whether multiple slip zones are active contemporaneously.

References

Aksu, A., Calon, T., and Hiscott, R.: Anatomy of the North Anatolian Fault Zone in the Marmara Sea, Western Turkey: Extensional basins above a continental transform, GSA Today, 6, 3 – 7, 2000.

Anders, M. and Wiltschko, D.: Microfracturing, paleostress and the growth of faults, Journal of Structural Geology, 16, 795 – 815, 1994.

585 Antonellini, M. and Aydin, A.: Effect of faulting on fluid flow in porous sandstones: Petrophysical properties, AAPG Bulletin, 78, 355 – 377, 1994.

Barth, N., Toy, V., Langridge, R., and Norris, R.: Scale dependence of oblique plate-boundary partitioning: New insights from LiDAR, central Alpine Fault, New Zealand, Lithosphere, 4, 435 – 448, https://doi.org/10.1130/L201.1, 2012.

Barth, N., Boulton, C., Carpenter, B., Batt, G., and Toy, V.: Slip localization on the southern Alpine Fault, New Zealand, Tectonics, 32, 620

590 – 640, https://doi.org/10.1002/tect.20041, 2013.

Beavan, J., Ellis, S., Wallace, L., and Denys, P.: Kinematic constraints from GPS on oblique convergence of the Pacific and Australian plates, central South Island, New Zealand, In: Okaya, D., Stern, T.A. and Davey, F. (eds.): A continental plate boundary: Tectonics at South Island, New Zealand. AGU Geophysical Monograph, 175, 75 – 94, 2007.

Ben-Zion, Y.: Collective behavior of earthquakes and faults: Continuum-discrete transitions, progressive evolutionary changes, and different

595 dynamic regimes, Reviews of Geophysics, 46, https://doi.org/10.1029/2008RG000260, 2008.

Ben-Zion, Y. and Sammis, C.: Characterization of fault zones, Pure and Applied Geophysics, 160, 677 – 715, 2003.

Biegel, R. and Sammis, C.: Relating fault mechanics to fault zone structures, Advances in Geophysics, 47, 65 – 111, 2004.

Blenkinsop, T.: Thickness-displacement relationships for deformation zones: Discussion, Journal of Structural Geology, 11, 1051 – 1054, 1989.

600 Boese, C., Townend, J., Smith, E., and Stern, T.: Microseismicity and stress in the vicinity of the Alpine Fault, central southern Alps, New Zealand, Journal of Geophysical Research, 117, https://doi.org/10.1029/2011JB008460, 2012.

Bohnhoff, M., Martínez-Garzón, P., Bulut, F., Stierle, E., and Ben-Zion, Y.: Maximum earthquake magnitudes along different sections of the North Anatolian Fault Zone, Tectonophysics, 674, 147 – 165, https://doi.org/10.1016/j.tecto.2016.02.028, 2016.

Boulton, C., Carpenter, B., Toy, V., and Marone, C.: Physical properties of surface outcrop cataclastic fault rocks, Alpine Fault, New Zealand,

605 Geochemistry, Geophysics, Geosystems, 13, 238 – 265, https://doi.org/10.1029/2011GC003872, 2012.

Boulton, C., Moore, D., Lockner, D., Toy, V., Townend, J., and Sutherland, R.: Frictional properties of exhumed fault gouges in DFDP-1 cores, Alpine Fault, Geophysical Research Letters, 41, 356 – 362, https://doi.org/10.1002/2013GL058236, 2014.

Boutareaud, S., Calugaru, D.-G., Han, R., Fabbri, O., Mizoguchi, K., Tsutsumi, A., and Shimamoto, T.: Clay-clast aggregates: a new textural evidence for seismic fault sliding?, Geophysical Research Letters, 35, https://doi.org/10.1029/2007GL032554, 2008.

610 Bruhn, R., Parry, W., Yonkee, W., and Thompson, T.: Fracturing and hydrothermal alteration in normal fault zones, Pure and Applied Geophysics, 142, 609 – 644, 1994.

Bürgmann, R. and Dresen, G.: Rheology of the lower crust and upper mantle: Evidence from rock mechanics, geodesy and field observations, Annual Reviews of Earth and Planetary Sciences, 36, 531 – 567, https://doi.org/10.1146/annurev.earth.36.031207.124326, 2008.

Caine, J., Evans, J., and Forster, C.: Fault zone architecture and permeability structure, Geology, 24, 1025 – 1028, 1996.

615 Carpenter, B., Kitajima, H., Sutherland, R., Townend, J., Toy, V., and Saffer, D.: Hydraulic and acoustic properties of the active Alpine Fault, New Zealand: Laboratory measurements on DFDP-1 drill core, Earth and Planetary Science Letters, 390, 45 – 51, https://doi.org/10.1016/j.epsl.2013.12.023, 2014.

Carpenter, B., Saffer, D., and Marone, C.: Composition, alteration, and texture of fault-related rocks from SAFOD core and surface outcrop analogs: evidence for deformation processes and fluid-rock interaction, Pure and Applied Geophysics, 172, 5273 – 5289, https://doi.org/10.1002/ 2015JB011963, 2015.

620 Chester, F. and Logan, J.: Implications for mechanical properties of brittle faults from observations of the Punchbowl Fault Zone, California, Pure and Applied Geophysics, 124, 79 – 106, 1986.

Chester, F., Evans, J., and Biegel, R.: Internal structure and weakening mechanisms of the San Andreas Fault, Journal of Geophysical Research, 98, 771 – 786, 1993.

625 Chester, J., Chester, F., and Kronenberg, A.: Fracture surface energy of the Punchbowl Fault, San Andreas System, Nature Letters, 437, 133 – 136, https://doi.org/10.1038/nature03942, 2005.

Columbus, J., Sirguey, P., and Tenzer, R.: A free fully assessed 15 meter digital elevation model for New Zealand, Survey Quarterly, 66, 16 – 19, 2011.

Cooper, A. and Norris, R.: Inverted metamorphic sequences in Alpine Fault mylonites produced by oblique shear within a plate boundary 630 fault zone, New Zealand, Geology, 39, 1023 – 1026, 2011.

Cowan, D., Cladouhos, T., and Morgan, J.: Structural geology and kinematic history of rocks formed along low-angle normal faults, Death Valley, California, GSA Bulletin, 115, 1230 – 1248, 2003.

Cox, S., Etheridge, M., and Wall, V.: The role of fluids in syntectonic mass transport and the localization of metamorphic vein-type ore deposits, Ore Geology Reviews, 2, 65 – 86, 1986.

635 Czaplinska, D., Piazolo, S., and Zibra, I.: The influence of phase and grain size distribution on the dynamics of strain localization in polymin-eralic rocks, Journal of Structural Geology, 72, 15 – 32, https://doi.org/10.1016/j.jsg.2015.01.001, 2015.

DeMets, C., Gordon, R., and Argus, D.: Geologically current plate motion, Geophysical Journal International, 181, 1 – 80, https://doi.org/10.1111/j.1365-246X.2009.04491.x, 2010.

Döbelin, N. and Kleeberg, R.: Profex: A graphical user interface for the Rietveld refinement program BGMN, Journal of Applied Crystal-640 lography, 48, 1573 – 1580, https://doi.org/10.1107/S16000576715014685, 2015.

Edbrooke, S., Hern, D., Forsyth, P., and Jongens, R.: Geological Map of New Zealand 1:1,000,000, GNS Science Geological Map 2. Lower Hut, New Zealand. GNS Science, 2015.

Eguchi, R., Goltz, J., Taylor, C., Chang, S., Flores, P., Johnson, L., Seligson, H., and Blais, N.: Direct economic losses in the Northridge Earthquake: A three-year post-event perspective, Earthquake Spectra, 14, 245 – 264, 1998.

645 Evans, J.: Thickness-displacement relationships for fault zones, Journal of Structural Geology, 12, 1061 – 1065, 1990.

Fagereng, A., Remitti, F., and Sibson, R.: Shear veins observed within anisotropic fabric at high angles to the maximum compressive stress, Nature Geoscience, 3, 482 – 485, https://doi.org/10.1038/NGE898, 2010.

Faulkner, D., Lewis, A., and Rutter, E.: On the internal structure and mechanics of large strike-slip fault zones: field observations of the Carboneras Fault in southeastern Spain, Tectonophysics, 367, 235 – 251, https://doi.org/10.1016/S0040-1951(03)00134-3, 2003.

650 Faulkner, D., Mitchell, T., Healy, D., and Heap, M.: Slip on 'weak' faults by the rotation of regional stress in the fracture damage zone, Nature Letters, 444, 922 – 925, https://doi.org/10.1038/nature05353, 2006.

Faulkner, D., C.A.L., J., Lunn, R., Schlische, R., Shipton, Z., Wibberley, C., and Withjack, M.: A review of recent developments concerning the structure, mechanics and fluid flow properties of fault zones, Journal of Structural Geology, 32, 1557 – 1575, https://doi.org/10.1016/j.jsg.2010.06.009, 2010.

655 Fossen, H.: Structural Geology, Cambridge University Press, 2nd edn., 2016.

Fossen, H. and Cavalcante, G.: Shear zones - A review, Earth-Science Reviews, 171, 434 – 455, https://doi.org/10.1016/j.earscirev.2017.05.002, 2017.

Grant, J.: The Isocon Diagram – a simple solution to Gresens' equation for metasomatic alteration, Economic Geology, 81, 1976 – 1982, 1986.

660 Grant, J.: Isocon analysis: a brief review of the method and applications, Physics and Chemistry of the Earth, 30, 997 – 1004, https://doi.org/10.1016/j.pce.2004.11.003, 2005.

Grapes, R. and Watanabe, T.: Metamorphism and uplift of Alpine Schist in the Franz Josef - Fox Glacier area of the Southern Alp, New Zealand, Journal of Metamorphic Geology, 10, 171 – 180, 1992.

Gresens, R.: Composition-volume relationships of metasomatism, Chemical Geology, 2, 47 – 65, 1967.

665 Haines, S. and van der Pluijm, B.: Clay quantification and Ar–Ar dating of synthetic and natural gouge: Application to the Miocene Sierra Mazatán Detachment Fault, Sonora, Mexico, Journal of Structural Geology, 30, 525 – 538, https://doi.org/10.1016/j.jsg.2007.11.012, 2008.

Hickman, S., Sibson, R., and Bruhn, R.: Introduction to special section: mechanical involvement of fluids in faulting, Journal of Geophysical Research, 100, 12 831 – 12 840, 1995.

670 Hobbs, B., Mühlhaus, H.-B., and Ord, A.: Instability, softening and localization of deformation, In: Knipe, R.J. and Rutter, E.H. (eds.): Deformation Mechanisms, Rheology and Tectonics, Geological Society Special Publication, 54, 143 – 165, 1990.

Holdsworth, R., van Diggelen, E., Spiers, C., de Bresser, J., Walker, R., and Bowen, L.: Fault rocks from the SAFOD core samples: implications for weakening at shallow depths along the San Andreas Fault, California, Journal of Structural Geology, 33, 132 – 144, https://doi.org/10.1016/j.jsg.2010.11.010, 2011.

675 Hollingsworth, J., L., Y., and Avouac, J.-P.: Dynamically triggered slip on a splay fault in the M_W 7.8, 2016 Kaikoura (New Zealand) earthquake, Geophysical Research Letters, 44, 3517 – 3525, https://doi.org/10.1002/2016GL072228, 2017.

Howarth, J., Cochran, U., Langridge, R., Clark, K., Fitzsimons, S., Berryman, K., Villamor, P., and Strong, D.: Past large earthquakes on the Alpine Fault: paleoseismological progress and future directions, New Zealand Journal of Geology and Geophysics, 61, 309 – 328, https://doi.org/10.1080/00288306.2018.1464658, 2018.

680 Hull, J.: Thickness-displacement relationships for deformation zones, Journal of Structural Geology, 10, 431 – 435, 1988.

Janku-Capova, L., Sutherland, R., Townend, J., Doan, M.-L., Massiot, C., Coussens, J., and Célérier, B.: Fluid flux in fractured rock of the Alpine Fault hanging-wall determined from temperature logs in the DFDP-2B borehole, New Zealand, Geochemistry, Geophysics, Geosystems, 9, https://doi.org/10.1029/2017GV007317, 2018.

Janssen, C., Laube, N., Bau, M., and Gray, D.: Fluid regime in faulting deformation of the Waratah Fault Zone, Australia, as inferred from 685 major and minor element analyses and stable isotopic signatures, Tectonophysics, 204, 109 – 130, 1998.

Janssen, C., Wirth, R., Wenk, H.-R., Morales, L., Naumann, R., Kienast, M., Song, S.-R., and Dresen, G.: Faulting processes in active faults - evidences from TCDP and SAFOD drill core samples, Journal of Structural Geology, 65, 100 – 116, https://doi.org/10.1016/j.jsg.2014.04.004, 2014.

Laurich, B., Urai, J., and Nussbaum, J.: Microstructures and deformation mechanisms in Opalinus Clay: insights from scaly clay from the 690 Main Fault in the Mont Terri Rock Laboratory (CH), Solid Earth, 8, 27 – 44, https://doi.org/19.5194/se-8-27-2017, 2017.

Laurich, B., Urai, J., Vollmer, C., and Nussbaum, C.: Deformation mechanisms and evolution of the microstructure of gouge in the Main Fault in Opalinus Clay in the Mont Terri Rock Laboratory (CH), Solid Earth, 9, 1 – 24, https://doi.org/10.5194/se-9-1-2018, 2018.

Lay, V., Buske, S., Lukács, A., Gorman, A., Bannister, S., and Schmitt, D.: Advanced seismic imaging techniques characterize the Alpine Fault at Whataroa (New Zealand), Journal of Geophysical Research: Solid Earth, 121, https://doi.org/10.1002/2016JB013534, 2016.

695 Li, H., Wang, H., Xu, Z., Si, J., Pei, J., Li, T., Huang, Y., Song, S.-R., Kuo, L.-W., Sun, Z., Chevalier, M.-L., and Liu, D.: Characteristics of the fault-related rocks, fault zones and the principal slip zone in the Wenchuan Earthquake Fault Scientific Drilling Project Hole-1 (WFSD-1), Tectonophysics, 584, 23 – 42, https://doi.org/10.1016/j.tecto.2012.08.021, 2013.

Lindsey, E., Fialko, Y., Bock, Y., Sandwell, D., and Bilham, R.: Localized and distributed creep along the southern San Andreas Fault, Journal of Geophysical Research: Solid Earth, 119, 7909 – 7922, https://doi.org/10.1002/2014JB011275, 2014.

700 Little, T., Cox, S., Vry, J., and Batt, G.: Variations in exhumation level and uplift rate along the oblique-slip Alpine Fault, central Southern Alps, New Zealand, GSA Bulletin, 117, 707 – 723, https://doi.org/10.1130/B25500.1, 2005.

Lockner, D., Morrow, C., Moore, D., and Hickman, S.: Low strength of deep San Andreas Fault gouge from SAFOD core, Nature, 472, 82 – 86, https://doi.org/10.1038/nature09927, 2011.

Lukács, A., Gorman, A., and Norris, R.: Quaternary structural and paleo-environmental evolution of the Alpine Fault near Haast,
705 New Zealand, from 2D seismic reflection and gravity data, New Zealand Journal of Geology and Geophyics, 31, 181 – 213, https://doi.org/10.1080/00288306.2018.1544153, 2018.

Ma, K., Tanaka, H., Song, S.-R., Wang, C.-Y., Hung, J.-H., Tsai, Y.-B., Mori, J., Song, Y., Yeh, E., Soh, W., Sone, H., Kuo, L.-W., and Wu, H.-Y.: Slip zone and energetics of a large earthquake from the Taiwan Chelungpu-fault Drilling Project, Nature, 444, 473 – 475, https://doi.org/10.1038/nature05253, 2006.

710 Martínez-Garzón, P., Bohnhoff, M., Ben-Zion, Y., and Dresen, G.: Scaling of maximum observed magnitudes with geometrical and stress properties of strike-slip faults, Geophysical Research Letters, 42, https://doi.org/10.1093/gji/ggx169, 2015.

Massiot, C., Célérier, B., Doan, M.-L., Little, T., Townend, J., McNamara, D., Williams, J., Schmitt, D., Toy, V., Sutherland, R., Janku-Capova, L., Upton, P., and Pezard, P.: The Alpine Fault hanging-wall viewed from within: Structural analysis of ultrasonic image logs in the DFDP-2B borehole, New Zealand, Geochemistry, Geophysics, Geosystems, 19, https://doi.org/10.1029/2017GC007368, 2018.

715 Menzies, C., Teagle, D., Niedermann, S., Cox, S., Craw, D., Zimmer, M., Cooper, M., and Erzinger, J.: Frictional strength of wet and dry montmorillonite, Earth and Planetary Science Letters, 455, 125 – 135, https://doi.org/10.1016/j.epsl.2016.03.046, 2016.

Mitchel, T. and Faulkner, D.: The nature and origin of off-fault damage surrounding strike-slip fault zones with a wide range of displacements: A field study from the Atacama fault system, northern Chile, Journal of Structural Geology, 31, 802 – 816, 2009.

Moore, D. and Lockner, D.: Friction of smectite clay montmorillonite, in: The Seismogenic Zone of Subduction Thrust Faults, p. 317–345,
720 Columbia University Press, 2007.

Moore, D. and Reynolds, Jr., R.: X-Ray Diffraction and the Identification of clay Minerals, Oxford University Press, Oxford, 1997.

Moore, D. and Rymer, M.: Talc-bearing serpentinite and the creeping section of the San Andreas Fault, Nature, 448, 795 – 797, https://doi.org/10.1038/nature06064, 2007.

Moore, D. and Rymer, M.: Correlation of clayey gouge in a surface exposure of serpentinite in the San Andreas Fault with gouge from the
725 San Andreas Fault Observatory at Depth (SAFOD), Journal of Structural Geology, 38, 51 – 60, https://doi.org/10.1016/j.jsg.2011.11.014, 2012.

Moore, D., Lockner, D., Shengli, M., Summers, R., and Byerlee, J.: Strength of serpentinite gouges at elevated temperatures, Journal of Geophysical Research, 102, 14 787 – 14 801, https://doi.org/10.1029/2010GL046129, 1997.

Nardini, L., Rybacki, E., Döhmann, M., Morales, L., Brune, S., and Dresen, G.: High-temperature shear zone formation in Carrara marble:
730 The effect of loading conditions, Tectonophysics, 749, 120 – 139, https://doi.org/10.1016/j.tecto.2018.10.022, 2018.

Nicol, A., Robinson, R., Van Dissen, R., and Harvison, A.: Variability of recurrence interval and single-event slip for surface-rupturing earthquakes in New Zealand, New Zealand Journal of Geology and Geophysics, 59, 97 – 116, https://doi.org/10.1080/00288306.2015.1127822, 2016.

Norris, R. and Cooper, A.: Origin of small-scale segmentation and transpressional thrusting along the Alpine Fault, New Zealand, GSA Bulletin, 107, 231 – 240, 1995.

Norris, R. and Cooper, A.: Erosional control on the structural evolution of a transpressional thrust complex on the Alpine Fault, New Zealand, Journal of Structural Geology, 19, 1323 – 1342, 1997.

Norris, R. and Cooper, A.: Late Quaternary slip rates and slip partitioning on the Alpine Fault, New Zealand, Journal of Structural Geology, 23, 507 – 520, https://doi.org/10.1002/2016JB013658, 2000.

Norris, R. and Cooper, A.: Very high strains recorded in mylonites along the Alpine Fault, New Zealand: Implications for the deep structure of plate boundary faults, Journal of Structural Geology, 25, 2141 – 2157, 2003.

Norris, R. and Cooper, A.: The Alpine Fault, New Zealand: Surface geology and field relationships, In: Okaya, D., Stern, T.A. and Davey, F. (eds.): A continental plate boundary: Tectonics at South Island, New Zealand. AGU Geophysical Monograph, 175, 157 – 175, 2007.

Norris, R. and Toy, V.: Continental transforms: A view from the Alpine Fault, Journal of Structural Geology, 64, 3 – 31, https://doi.org/10.1016/j.jsg.2014.03.003, 2014.

Passchier, C. and Trouw, R.: Microtectonics, Springer, 2nd edn., 2005.

Peacock, D., Nixon, C., Rotevatn, A., Sanderson, D., and Zuluaga, L.: Glossary of fault and other fracture networks, Journal of Structural Geology, 92, 12 – 29, https://doi.org/10.1016/j.jsg.2016.09.008, 2016.

Reed, J.: Myonites, cataclasites, and associated rocks along the Alpine Fault, South Island, New Zealand, New Zealand Journal of Geology and Geophysics, 7, 645 – 684, https://doi.org/10.1080/00288306.1964.10428124, 1964.

Roser, B. and Cooper, A.: Geochemistry and terrane affiliation of Haast schist from the western southern Alps, New Zealand, New Zealand Journal of Geology and Geophysics, 33, 1 – 10, https://doi.org/10.1080/00288306.1990.10427567, 1990.

Rybacki, E., Janssen, C., Wirth, R., Chen, K., Wenk, H.-R., Stromeyer, D., and Dresen, G.: Low-temperature deformation in calcite veins of SAFOD core samples (San Andreas Fault) – microstructural analysis and implications for fault rheology, Tectonophysics, 509, 107 – 119, https://doi.org/10.1016/j.tecto.2011.05.014, 2011.

Rybacki, E., Morales, L., Naumann, M., and Dresen, G.: Strain localization during high temperature creep of marble: The effect of inclusions, Tectonophysics, 634, 182 – 197, https://doi.org/10.1016/j.tecto.2014.07.032, 2014.

Sahin, M. and Tari, E.: The August 17 Kocaeli and the November 12 Düzce earthquakes in Turkey, Earth Planets Space, 52, 753 – 757, https://doi.org/10.1016/j.tecto.2011.05.014, 2000.

Schindelin, J., Arganda-Carreras, I., Frise, E., Kaynig, V., Longair, M., Pietzsch, T., Preibisch, S., Rueden, C., Saalfeld, S., Schmid, B., Tinevez, J.-Y., White, D., Hartenstein, V., Eliceiri, K., Tomancak, P., and Cardona, A.: Fiji: an open-source platform for biological-image analysis, Nature methods, 9, 676 – 682, 2012.

Schleicher, A., Tourscher, S., van der Pluijm, B., and Warr, L.N.: Constraints on mineralization, fluid-rock interaction, and mass transfer during faulting at 2 – 3 km depth from the SAFOD drill hole, Journal of Geophysical Research, 114, https://doi.org/10.1029/2008JB006092, 2009.

Schleicher, A., van der Pluijm, B., and Warr, L.N.: Nanocoatings of clay and creep of the San Andreas Fault at Parkfield, Geology, 38, 667 – 670, https://doi.org/10.1130/G31091.1, 2010.

Schleicher, A., Sutherland, R., Townend, J., Toy, V., and van der Pluijm, B.: Clay mineral formation and fabric development in the DFDP-1B borehole, central Alpine Fault, New Zealand, New Zealand Journal of Geology and Geophysics, 58, 13 – 21, https://doi.org/10.1080/00288306.2014.979841, 2015.

Schneider, C., Rasband, W., and Eliceiri, K.: NIH Image to ImageJ: 25 years of image analysis, Nature methods, 9, 671 – 675, 2012.

Scholz, C.: Wear and gouge formation in brittle faulting, Geology, 15, 493 – 495, 1987.

Schrank, C., Handy, M., and Fusseis, F.: Multiscaling of shear zones and the evolution of the brittle-to-viscous transition in continental crust, Journal of Geophysical Research, 113, https://doi.org/10.1029/2006JB004833, 2008.

Schuck, B., Janssen, C., Schleicher, A., Toy, V., and Dresen, G.: Microstructures imply cataclasis and authigenic mineral formation control geomechanical properties of New Zealand's Alpine Fault, Journal of Structural Geology, 110, 172 – 186, https://doi.org/10.1016/jsg.2018.03.001, 2018.

Scott, J., Auer, A., Muhling, J., Czertowicz, T., Cooper, A., Billia, M., and Kennedy, A.: New P-T and U-Pb constraints on Alpine Schist metamorphism in south Westland, New Zealand, New Zealand Journal of Geology and Geophysics, 58, 385 – 397, https://doi.org/10.1080/00288306.2015.1093005, 2015.

Segall, P. and Pollard, D.: Nucleation and growth of strike slip faults in granite, Journal of Geophysical Research, 88, 555 – 568, https://doi.org/10.1080/00288306.2015.1093005, 1983.

Sibson, R.: A note on fault reactivation, Journal of Structural Geology, 7, 751 – 754, 1985.

Sibson, R.: Thickness of the Seismic Slip Zone, Bulletin of the Seismological Society of America, 93, 1169 – 1178, 2003.

Sibson, R., White, S., and Atkinson, B.: Fault rock distribution and structure within the Alpine Fault Zone: A preliminary account, In: Walcott, R.I. and Cresswell, M.M. (eds.): The origin of the Southern Alps. Bulletin of the Royal Society of New Zealand, 18, 55 – 65, 1979.

Spandler, C., Worden, K., Arculus, R., and Eggins, S.: Igneous rocks of the Brook Street Terrane, New Zealand: implications for Permian tectonics of eastern Gondwana and magma genesis in modern intra-oceanic volcanic arcs, New Zealand Journal of Geology and Geophysics, 48, 167 – 183, 2005.

Stern, T., Kleffmann, S., Okaya, D., Scherwath, M., and Bannister, S.: Low seismic-wave speeds and enhanced fluid pressure beneath the Southern Alps of New Zealand, Geology, 29, 679 – 682, 2001.

Sutherland, R., Eberhart-Phillips, D., Harris, R., Stern, T., Beavan, J., Ellis, S., Henrys, S., Cox, S., Norris, R., Berryman, K., Townend, J., Bannister, S., Pettinga, J., Leitner, B., Wallace, L., Little, T., Cooper, A., Yetton, M., and Stirling, M.: Do great earthquakes occur on the Alpine Fault in central South Island, New Zealand?, In: Okaya, D., Stern, T.A. and Davey, F. (eds.): A continental plate boundary: Tectonics at South Island, New Zealand. AGU Geophysical Monograph, 175, 235 – 251, 2007.

Sutherland, R., Toy, V., Townend, J., Cox, S., Eccles, J., Faulkner, D., Prior, D., Norris, R., Mariani, E., Boulton, C., Carpenter, B., Menzies, C., Little, T., Hasting, M., De Pascale, G., Langridge, R., Scott, H., Lindroos, Z., Fleming, B., and Kopf, A.: Drilling reveals fluid control on architecture and rupture of the Alpine Fault, New Zealand, Geology, 40, 1143 – 1146, https://doi.org/10.1130/G33614.1, 2012.

Sutherland, R., Townend, J., Toy, V., Allen, M., Baratin, L., Barth, N., Becroft, L., Benson, l., Boese, C., Boles, A., Boulton, C., Capova, l., Carpenter, B., Célérier, B., Chamberlain, C., Conze, R., Cooper, A., Coussens, J., Coutts, A., Cox, S., Craw, L., Doan, M., Eccles, J., Faulkner, D., Grieve, J., Grochowski, J., Gulley, A., Henry, G., Howarth, J., Jacobs, K., Jeppson, T., Kato, N., Keys, S., Kirilova, M., Kometani, Y., Kovacs, A., Langridge, R., Lin, W., Little, T., Mallyon, D., Mariani, B., Marx, R., Massiot, C., Mathewson, L., Melosh, B., Menzies, C., Moore, J., Morales, L., Morgan, C., Mori, H., Niemeijer, A., Nishikawa, O., Nitsch, O., Paris Cavailhès, J., Pooley, B., Prior, D., Pyne, A., Sauer, K., Savage, M., Schleicher, A., Schmitt, D., Shigematsu, N., Taylor-Offord, S., Tobin, H., Upton, P., Valdez, R.,

Weaver, K., Wiersberg, T., J., W., Yeo, S., and Zimmer, M.: Deep Fault Drilling Project (DFDP), Alpine Fault Boreholes DFDP-2A and DFDP-2B Technical Completion Report, GNS Science Report 2015/50, 2015.

Sutherland, R., Townend, J., Toy, V., Upton, P., Coussens, J., Allen, M., Baratin, L.-M., Barth, N., Becroft, L., Boese, C., Boles, A., Boulton, C., Broderick, N., Janku-Capova, L., Carpenter, B., Célérier, B., Chamberlain, C., Cooper, A., Coutts, A., Cox, S., Craw, L., Doan, M.-L., Eccles, J., Faulkner, D., Grieve, J., Grochowski, J., Gulley, A., Hartog, A., Howarth, J., Jacobs, K., Jeppson, T., Kato, N., Keys, S., Kirilova, M., Kometani, Y., Langridge, R., Lin, W., Little, T., Lukacs, A., Mallyon, D., Mariani, E., Massiot, C., Mathewson, L., Melosh, B., Menzies, C., Moore, J., Morales, L., Morgan, C., Mori, H., Niemeijer, A., Nishikawa, O., Prior, D., Sauer, K., Savage, M., Schleicher, A., Schmitt, D., Shigematsu, N., Taylor-Offord, S., Teagle, D., Tobin, H., Valdez, R., Weaver, K., Wiersberg, T., Williams, J., Woodman, N., and Zimmer, M.: Extreme hydrothermal conditions at an active plate-bounding fault, Nature, 545, https://doi.org/doi: 10.1038/nature22355, 2017.

Toby, B.: R factors in Rietveld analysis: How good is good enough?, Powder Diffraction, 21, 67 – 70, 2006.

Toppozada, T., D.M., B., Reichle, M., and Hallstrom, C. L.: San Andreas Fault Zone, California: M geq 5.5 earthquake history, Bulletin of the Seismological Society of America, 92, 2555 – 2601, 2002.

Townend, J. and Zoback, M.: How faulting keeps the crust strong, Geology, 28, 399 – 402, 2000.

Townend, J., Sutherland, R., and Toy, V.: Deep Fault Drilling Project - Alpine Fault, New Zealand, Scientific Drilling, 8, 75 – 82, 2009.

Townend, J., Sutherland, R., Toy, V., Eccles, J., Boulton, C., Cox, S., and McNamara, D.: Late-interseismic state of a continental plate-bounding fault: Petrophysical results from DFDP-1 wireline logging and core analysis, Alpine Fault, New Zealand, Geochemistry, Geophysics, Geosystems, 14, 3801 – 3820, https://doi.org/10.1002/ggge.20236, 2013.

Townend, J., Sutherland, R., Toy, V., Doan, M.-L., Célérier, B., Massiot, C., Coussens, J., Jeppson, T., Janku-Capova, L., Remaud, L., Upton, P., Schmitt, D., Williams, J., Allen, M., Baratin, L.-M., Barth, N., Becroft, L., Boese, C., Boulton, C., Broderick, N., Carpenter, B., Chamberlain, C., Cooper, A., Coutts, A., Cox, S., Craw, L., Eccles, J., Faulkner, D., Grieve, J., Grochowski, J., Gulley, A., Hartog, A., Henry, G., Howarth, J., Jacobs, K., Kato, N., Keys, S., Kirilova, M., Kometani, Y., Langridge, R., Lin, W., Little, T., Lukacs, A., Mallyon, D., Mariani, E., Mathewson, L., Melosh, B., Menzies, C., Moore, J., Morales, L., Mori, H., Niemeijer, A., Nishikawa, O., Nitsch, O., Paris, J., Prior, D., Sauer, K., Savage, M., Schleicher, A., Shigematsu, N., Taylor-Offord, S., Teagle, D., Tobin, H., Valdez, R., Weaver, K., Wiersberg, T., and Zimmer, M.: Petrophysical, geochemical, and hydrological evidence for extensive fracture-mediated fluid and heat transport in the Alpine Fault's hanging-wall damage zone, Geochemistry, Geophysics, Geosystems, 18, 4709 – 4732, https://doi.org/10.1002/2017GC007202, 2017.

Toy, V., Norris, R., Prior, D., Walrond, M., and Cooper, A.: How do lineations reflect the strain history of transpressive shear zones? The example of the active Alpine Fault Zone, New Zealand, Journal of Structural Geology, 50, 187 – 198, https://doi.org/10.1016/j.jsg.2012.06.006, 2013.

Toy, V., Boulton, C., Sutherland, R., Townend, J., Norris, R., Little, T., Prior, D., Mariani, E., Faulkner, D., Menzies, C., Scott, H., and Carpenter, B.: Fault rock lithologies and architecture of the central Alpine Fault, New Zealand, revealed by DFDP-1 drilling, Lithosphere, 7, 155 – 173, https://doi.org/10.1130/L395.1, 2015.

Toy, V., Sutherland, R., Townend, J., Allen, M., Becroft, L., Boles, A., Boulton, C., Carpenter, B., Cooper, A., Cox, S., Daube, C., Faulkner, D., Halfpenny, A., Kato, N., Keys, S., Kirilova, M., Kometani, Y., Little, T., Mariani, E., Melosh, B., Menzies, C., Morales, L., Morgan, C., Mori, H., Niemeijer, A., Norris, R., Prior, D., Sauer, K., Schleicher, A., Shigematsu, N., Teagle, D., Tobin, H., Valdez, R., Williams, J., Yea, S., Baratin, L.-M., Barth, N., Benson, A., Boese, C., Célérier, B., Chamberlain, C., Conze, R., Coussens, J., Craw, L., Doan, M.-L., Eccles, J., Grieve, J., Grochowski, J., Gulley, A., Howarth, J., Jacobs, K., Janku-Capova, L., Jeppson, T., Langridge, R., Mallyon,

D., Marx, R., Massiot, C., Mathewson, L., Moore, J., Nishikawa, O., Pooley, B., Pyne, A., Savage, M., Schmitt, D., Taylor-Offord, S.,
845   Upton, P., Weaver, K., Wiersberg, T., Zimmer, M., and DFDP-2 Science Team: Bedrock geology of DFDP-2B, central Alpine Fault, New
       Zealand, New Zealand Journal of Geology and Geophysics, https://doi.org/10.1080/00288306.2017.1375533, 2017.

Twiss, R. and Moores, E.: Structural Geology, W.H. Freeman and Company, 2nd edn., 2007.

Van Eijs, R., Mulders, F., Nepveu, M., Kenter, C., and Scheffers, B.: Correlation between hydrocarbon reservoir properties and induced
       seismicity in the Netherlands, Engineering Geology, 84, 99 – 111, https://doi.org/19.1016/j.enggeo.2006.01.002, 2006.

850   Vannucchi, O., Maltman, A., Bettelli, G., and Clennell, B.: On the nature of scaly fabric and scaly clay, Journal of Structural Geology, 25,
       673 – 688, 2003.

Warr, L. and Cox, S.: Clay mineral transformations and weakening mechanisms along the Alpine Fault, New Zealand, In: Holdsworth, R.E.,
       Strachan, R.A., Magloughlin, J.F. and Knipe, R.J. (eds.): The nature and tectonic significance of fault zone weakening. Geological Society,
       London, Special Publications, 186, 85 – 101, 2001.

855   Warren-Smith, E., Lamb, S., and Stern, T.: Stress field and kinematics for diffuse microseismicity in a zone of continental transpression,
       South Island, New Zealand, Journal of Geophysical Research: Solid Earth, 122, https://doi.org/10.1002/2017JB013942, 2017.

Wibberley, C., Yielding, G., and Di Toro, G.: Recent advances in the understanding of fault zone internal structure: a review, In: Wibberley,
       C.A.J., Kurz W., Imber, J., Holdsworth, R.E. and Collettini, C. (eds.): The Internal Structure of Fault Zones: Implications for Mechanical
       and Fluid-Flow Properties. Geological Society, London, Special Publications, 299, 5 – 33, https://doi.org/10.1144/SP299.2, 2008.

860   Williams, J., Toy, V., Massiot, C., McNamara, D., and Wang, T.: Damaged beyond repair? Characterizing the damage zone of a fault late in its
       interseismic cycle, the Alpine Fault, New Zealand, Journal of Structural Geology, 90, 76 – 94, https://doi.org/10.1016/j.jsg.2016.07.006,
       2016.

Williams, J., Toy, V., Smith, S., and Boulton, C.: Fracturing, fluid-rock interaction and mineralization during the seismic cycle along the
       Alpine Fault, Journal of Structural Geology, 103, 151 – 166, https://doi.org/10.1016/j.jsg.2017.09.011, 2017.

865   Williams, J., Toy, V., Massiot, C., McNamara, D., Smith, S., and Mills, S.: Controls on fault zone structure and brittle fracturing in the
       foliated hanging wall of the Alpine Fault, Solid Earth, 9, 469 – 489, https://doi.org/10.5194/se-9-469-2018, 2018.

Wirth, R.: A novel technology for advanced application of micro- and nanoanalysis in geosciences and applied mineralogy, European Journal
       of Mineralogy, 16, 863 – 876, https://doi.org/10.1127/0935-1221/2004/0016-0863, 2004.

Wirth, R.: Focused Ion Beam (FIB) combined with SEM and TEM: advanced analytical tools for studies of chemical com-
870   position, microstructure and crystal structure in geomaterials on a nanometre scale, Chemical Geology, 261, 217 – 229,
       https://doi.org/10.1016/j.chemgeo.2008.05.019, 2009.

Zoback, M., Hickman, S., and Ellsworth, W.: The role of fault zone drilling, in: Treatise on geophysics, edited by Schubert, G., p. 649 – 674,
       Elsevier, Amsterdam, 2007.

Table 1: Summary of observed hanging-wall cataclasite microstructures. PSZ: principal slip zone.

	poor	localization	high
	DFDP-1A	**Waikukupa Thrust**	**Martyr River**
fractures	X	X	X
- amount increases towards PSZ	X	X	/
PSZ			
microfaults	~5 - 130 μm wide	~5 - 130 μm wide	/
detrital clasts			
- main phases	quartz & feldspar	quartz & feldspar	polymineralic aggregates (mainly quartz, feldspar & chlorite)
- minor phases	/	micas (elongated, kinked & fractured), hornblende & chlorite aggregates (up to 0.6 × 1 mm large)	quartz & feldspar (< 5 %)
- roundness	angular - rounded	angular - rounded	angular - rounded
- sphericity	low - moderate	low - moderate	low - moderate
- amount			
- PSZ-proximal	~ 50 % (at ~ 3 m above PSZ)	~ 60 - 70 % (at ~ 70 cm above PSZ)	not sampled
- at contact to PSZ	~ 10 %	~ 20 - 25 %	~ 40 - 50 %
- size			
- PSZ-proximal	~ 100s of μm (at ~ 3 m above PSZ)	~ 100s of μm (at ~ 70 cm above PSZ)	not sampled
- at contact to PSZ	~ 100 μm	~ 100 μm	~ 100 - 200 μm
- maximum	~ 550 × 600 μm	~ 550 × 600 μm	~ 200 μm
fragments			
- schist	1.6 × 3.4 mm large	2.8 × 5.4 mm large	1.1 mm large
- fractured & gouge-filled	X	X	/
- mylonite	/	9 - 12 mm large	/
- fractured & gouge-filled	X	X	/
matrix clasts			
- first observation	~ 1.35 m above PSZ	~ 10 cm above PSZ	/
- max. size	650 × 750 μm	1.3 × 3.4 mm	/
patches of authigenic	X	X	/
chlorite crystallites			
- amount increases towards PSZ	X	X	/
bright matrix clasts	X	X	X
calcite			
- occurrence	all samples	mostly in direct vicinity to PSZ	all samples
- kind: cement	within some fractures; local	within some fractures; generally insignificant; slightly more pronounced within ~ 3 cm of PSZ	within some fractures; finely-dispersed & abundant
- kind: lenses	up to 1.2 × 4 mm	/	/
- kind: veins	frequent with increasing abundance towards the PSZ; mostly restricted to clasts; up to 5 - 300 μm thick; typically between 50 - 70 μm thick	~ < 15 μm thick; mutually cross-cutting with small (< 20 μm), dextral offsets	/

	poor	localization	high
	DFDP-1A	Waikukupa Thrust	Martyr River
foliation	locally & weak; formed by clasts and microfaults; locally with SC-geometry	clast-lenses parallel to PSZ	/
other	/	breccias (< 100µm large) within some centimeters above the PSZ; clay-clast-aggregates	/

Solid Earth
Discussions
Open Access
EGU

Table 2: Summary of observed principal slip zone (fault gouge) microstructures. PSZ: principal slip zone; HW: hanging-wall; FW: footwall.

	poor	localization			high
	Havelock Creek	**Gaunt Creek**	**DFDP-1A**	**Waikukupa Thrust**	**Martyr River**
contact HW - PSZ	transitional over 8 cm	not sampled	not sampled	sharp at macro- & mesoscale; transitional over 4 mm at microscale & sharp at macro- & mesoscale; difficult to identify at microscale	
major differences compared to hanging-wall	not sampled	not sampled	~ 90 % of PSZ is cemented	FW-prox. gouge: dense anastomosing network of mutually cross-cutting calcite veins	I) clasts are small individual mineral phases and not chloritized aggregates; II) no calcite cement, but less porous due to authigenic phyllosilicates
kind of PSZ	single structure	single structure	single structure	layered HW-prox. gouge 2 cm thick FW-prox. gouge 2 cm thick	layered HW-prox. gouge 0.8 – 1 cm thick FW-prox. gouge 0.3 – 0.5 cm thick
- contact between PSZ layers	/	/	/	sharp & undulating & poorly developed at microscale	/
- major differences between PSZ layers	/	/	/	FW-prox. gouge hosts dense, anastomosing network of mutually cross-cutting calcite veins	20 - 25 % clasts in HW-prox. gouge vs. 25 - 30 % clasts in FW-prox. gouge
similarities between investigated PSZs	HW-prox. gouge at Waikukupa Thrust	FW-prox. gouge at Waikukupa Thrust	/	Havelock Creek (HW-prox. gouge); Gaunt Creek (FW-prox. gouge)	/
detrital clasts					
- main phases	quartz & feldspar	quartz & feldspar	quartz & feldspar	quartz & feldspar	quartz & feldspar
- minor phases	hornblende & mica fragments (50 × 350 µm large)	/	/	/	hornblende; mica fragments (<20 µm large) & needle-shaped serpentines (<20 µm large)
- roundness	(sub)angular - rounded	(sub)angular - rounded	(sub)angular - rounded	(sub)angular - rounded	(sub)angular - rounded
- sphericity	elongate - moderate	elongate - moderate	elongate - moderate	elongate - moderate	elongate - moderate
- amount	10 %	<1 %	/	HW-prox. gouge: 5 - 10 %; FW-prox. gouge: <1 %	20-30 %
- size	~ 75 µm	~ 15 µm	/	~ 100 µm; decreases towards FW	HW-prox. gouge 10s - 200 µm; FW-prox. gouge < 100 µm
- maximum	160 × 250 µm	90 × 130 µm	/	110 × 180 µm	1 mm
- fragments - kind	schist	/	/	/	schist, mylonite, cataclasite

	poor		localization		high
	Havelock Creek	**Gaunt Creek**	**DFDP-1A**	**Waikukupa Thrust**	**Martyr River**
- roundness	subangular - -rounded	/	/	/	subangular - -rounded
- sphericity	low - moderate	/	/	/	low - moderate
- size	15 - 50 µm	/	/	/	/ 100s of micrometer (schist)
- maximum	400 × 450 µm	/	/	/	>2.2 × 3.7 mm (schist); 3 × 7.5 mm (mylonite); 5 × 6 mm (cataclasite)
- other	/	/	/	clast size decreases towards FW	/
matrix clasts - maximum size	prevailing type of clast 650 × 830 µm	/	/	prevail at HW-prox. gouge 3 µm – >6 mm	< 5 % of clasts ~20 µm – 3 × 3.5 mm
patches of authigenic chlorite crystallites	/	/	associated with non-cemented fractures	/	/
bright matrix clasts - abundance	high	high	low (local)	/	low (local)
calcite veins	very rare	network	rarev	rare (HW-prox. gouge); network (FW-prox. gouge)	rare
- thickness - vein network	/	350 - 800 µm	/	~ 2 cm (FW-prox. gouge)	/
- individual veins	/	5 - 10 µm, up to 30 µm, increases slightly towards FW	up to 350 µm	HW-prox. gouge ~ 10 µm; FW-prox. gouge typically ~ 60 µm, between 1.5 - 200 µm decreases to FW	15 - 900 µm
- spacing	/	20 - 30 µm; between 10 - 80µm	/	200 µm (close to HW-prox. gouge), 10µm (close o FW)	/
- orientations	/	/	/ FW-prox. gouge; I) subparallel to displacement; II) oblique to displacement; III) normal to displacement	/	/
- CL color	/	mostly uniform yellow – orange; slightly brighter and more yellow to FW	/	uniform yellow – orange	/
- other	/	/	/	small (<5 µm), blocky & euhedral crystals	/
foliation	/	/	/	/	in HW-prox. gouge; weak; parallel to PSZ; formed by clasts
other	/	/	slickolite	HW-prox. gouge: CCAs & breccias (0.6 × 1.2 mm)	/

Solid Earth Discussions — Open Access EGU

Table 3: Summary of observed footwall (Quaternary gravel) microstructures. PSZ: principal slip zone; FW: footwall.

	poor	localization	high
	Gaunt Creek	**Waikukupa Thrust**	**Martyr River**
contact PSZ - FW	sharp	sharp	not sampled
detrital clasts			
- main phases	quartz & feldspar	quartz & feldspar	quartz & feldspar
- minor phases	mica	mica	mica, serpentine
- roundness	subangular - subrounded	subangular - subrounded / subangular - subrounded	subangular - subrounded
- sphericity	low - moderate	low - moderate	low - high
- amount	25 - 30 %	40 - 50 %	50 - 60 %
- size	~ 140 - 185 μm	~ 60 - 130 μm	~ 100 - 200 μm
- trend	/	increases with increasing distance to PSZ	increases with increasing distance to PSZ
- fragments	schist & cataclasite & schist, mylonite	cataclasite	schist & cataclasite
- maximum size			
- schist	~ 4.1 × 5.3 mm	~ 1 × 1.5 cm	0.7 × 1.4 cm
- mylonite	/	~ 0.7 cm	/
- cataclasite	~ 3.4 × 5.6 mm	0.5 - 0.7 cm	0.5 × 1.1 cm
matrix clasts	~ 300 μm (up to 4.3 × 7.4 mm)	/	/
patches of authigenic chlorite crystallites	X	/	/
bright matrix clasts			
- abundance	high	/	low
calcite			
- kind: cement		in general, mostly restricted to ~ 3 mm within contact to PSZ finely dispersed	
- kind: veins	up to ~ 350 μm thick; cross-cut detrital clasts	veinlets & a few displacement-normal veins extending from FW-prox. gouge into footwall	/
- kind: other	lenses (up to 1 × 1.4 mm large) within detrital clasts	calcite rims (<5 μm) at clasts parallel to displacement	/
foliation	/	/	weak; parallel to PSZ; formed by slightly imbricated clasts
other	0.75 - 1.6 cm thick lens of matrix clasts (size: ~100 - 300μm; up to 1.4 × 2.1 mm); fractures between individual clasts are gouge-filled; <5 % detrital clasts	/	/

Table 4. Mineralogical composition [wt%] of investigated samples as determined by XRD and subsequent Rietveld refinement. Mineral abbreviations are: Qtz: quartz; Plg: plagioclase; KFsp: potassium feldspar; Cc: calcite; Ank: ankerite; Chl: chlorite; Kln: kaolinite; Ms: muscovite; Ill: illite; Bt: biotite; Amp: amphibole; Ep: epidote; Srp: serpentine group minerals; Ap: apatite; Py: pyrite.

sample	location	lithology	dist. to PSZ[a]	Qtz	Plg[b]	KFsp	Cc	Ank	Chl	Kln	Ms	Ill	Bt	Amp[c]	Ep	Srp[d]	Ap	Py
129	Havelock Creek	gouge	0 cm	23	25	4	11		19	2	4	5	3	3				<1
130_1	Gaunt Creek	gouge	0 cm	22	14	7	6		6		46							
130_2	Gaunt Creek	gravel	-2.5 cm	23	21	7	6		12		3	25	2					
130_3	Gaunt Creek	gravel	-4.75 cm	25	20	15	6		8	1	14	6	5					
120	DFDP-1A	cataclasite	292 cm	32	9	4	3		10	1	20	14	7				<1	
119	DFDP-1A	cataclasite	270 cm	26	26	7	5		9	2	23		2				<1	
118	DFDP-1A	cataclasite	135 cm	29	7	4	2		14	22	18	3	<1				1	
117	DFDP-1A	cataclasite	87 cm	37	11	7	8		11	1	23	2	1					
116	DFDP-1A	cataclasite	25 cm	22	6	18	18		22	4	3	4	2				<1	
115	DFDP-1A	gouge	0 cm	27	8	5	2		5	30	10	11	2				<1	
132	Waikukupa Thrust	cataclasite	70 cm	23	41		3	1	16	<1	2		4	9				<1
124	Waikukupa Thrust	cataclasite	25 cm	29	36	1	2		9	1	1	1	2	12	6			<1
125_1	Waikukupa Thrust	cataclasite	8 cm	32	36	1	2		11	1	1		3	8	6			<1
131_2	Waikukupa Thrust	gouge	2 cm	22	17	4	16		10	1	28	<1	1	1			1	<1
131_1	Waikukupa Thrust	gouge	0 cm	11	8	2	29		5	1	<1	41	1				1	<1
133	Waikukupa Thrust	gravel	-10 cm	31	33	1	1	1	7		4	10	7	4	2			
127_3	Martyr River	cataclasite	2 cm	20	23	5	10		15	17	3	1	1		7			
127_4	Martyr River	gouge	0 cm	13	9	4	3		9	38	4	8	2			5	<1	

a) Datum to calculate distance to PSZ refers to center of PSZ at Martyr River, Havelock Creek and the DFDP-1A borehole and to the contact between PSZ and footwall at Waikukupa Thrust and Gaunt Creek.

b) Albite is the main plagioclase phase.

c) Amphibole minerals encountered are typically hornblende.

d) Main serpentine group minerals are to equal amounts lizardite and amesite.

Solid Earth
Discussions
Open Access
EGU

Table 5. Geochemical composition [wt%] of investigated samples as determined by XRF.

sample	location	lithology	dist. to PSZ[a]	MnO	P_2O_5	TiO_2	Na_2O	K_2O	CaO	MgO	Fe_2O_3[b]	Al_2O_3	SiO_2	LOI	total
129	Havelock Creek	gouge	0 cm	0.13	0.20	0.81	1.77	1.39	7.85	4.20	6.49	13.60	51.7	11.49	99.62
130_1		gouge	0 cm	0.13	0.19	0.76	1.94	3.27	6.78	3.64	6.66	13.43	51.40	11.38	99.58
130_2	Gaunt Creek	gravel	-2.5 cm	0.10	0.21	0.84	2.08	3.01	4.84	3.81	6.38	14.11	54.56	9.67	99.61
130_3		gravel	-4.75 cm	0.11	0.21	0.74	2.11	2.86	5.60	3.53	5.72	13.73	56.13	8.90	99.63
120		cataclasite	292 cm	0.06	0.17	0.70	1.15	4.20	1.94	3.01	5.66	16.12	60.54	6.08	99.63
119		cataclasite	270 cm	0.07	0.15	0.63	2.32	2.42	3.79	2.23	3.95	12.72	53.31	18.2	99.79
118	DFDP-1A	cataclasite	135 cm	0.04	0.17	0.58	1.19	4.17	1.76	2.52	4.20	14.31	65.95	4.88	99.76
117		cataclasite	87 cm	0.08	0.16	0.54	0.84	3.16	3.97	3.13	4.23	11.75	53.10	18.77	99.73
116		cataclasite	25 cm	0.17	0.18	0.71	0.38	3.56	10.99	4.48	5.70	11.64	44.66	17.15	99.62
115		cataclasite	0 cm	0.06	0.18	0.56	1.29	3.80	2.03	2.12	4.00	13.25	62.62	9.71	99.62
132		cataclasite	70 cm	0.13	0.11	0.89	4.20	0.52	3.74	4.93	7.73	14.37	59.25	3.77	99.64
124		cataclasite	25 cm	0.12	0.09	0.52	3.25	0.30	4.41	3.16	5.58	12.81	55.58	13.81	99.64
125_1	Waikukupa Thrust	cataclasite	8 cm	0.11	0.10	0.61	3.11	0.44	4.34	3.44	5.57	12.73	58.13	11.00	99.57
131_2		gouge	2 cm	0.15	0.16	0.72	1.38	2.11	10.09	2.98	6.15	12.75	50.31	14.73	101.53
131_1		gouge	0 cm	0.27	0.13	0.57	0.85	1.78	24.96	2.42	5.18	10.07	38.62	12.73	97.58
133		gravel	-10 cm	0.11	0.15	0.81	3.03	1.82	2.47	2.74	6.12	14.75	64.98	2.74	99.73
127_3	Martyr River	cataclasite	2 cm	0.11	0.18	0.69	2.27	1.80	8.74	4.50	6.11	13.45	52.67	8.96	99.47
127_4		gouge	0 cm	0.10	0.14	0.56	2.09	1.55	3.50	10.59	5.99	11.07	56.61	7.34	99.54

[a] Datum to calculate distance to PSZ refers to center of PSZ at Martyr River, Havelock Creek and the DFDP-1A borehole and to the contact between PSZ and footwall at Waikukupa Thrust and Gaunt Creek.

[b] Fe_2O_3 is total Fe content.

Table 6. Slope m of the isocon and derived mass change [%], enrichment (positive values) and depletion (negative values) of elements for samples investigated relative to the host rocks. Geochemical composition of fault rocks is taken from table 5 and composition of host rocks from Table S1. All concentrations are in wt%.

sample	location	unit	dist. to PSZ[a]	m	mass	MnO	P₂O₅	TiO₂	Na₂O	K₂O	CaO	MgO	Fe₂O₃[b]	Al₂O₃	SiO₂	LOI
129	Havelock Creek	gouge	0 cm	0.74	35.12	251.30	117.61	126.88	-21.93	-7.63	587.26	324.56	143.81	40.78	-2.71	489.55
130_1		gouge	0 cm	0.74	35.85	258.65	101.63	115.38	-13.97	118.48	496.81	269.95	151.56	39.77	-2.75	487.03
130_2	Gaunt Creek	gravel	-2.5 cm	0.78	28.45	167.18	110.93	125.06	-12.78	90.15	302.83	266.14	127.86	38.85	-2.40	371.55
130_3		gravel	-4.75 cm	0.80	25.34	180.77	102.86	93.24	-13.66	76.30	354.81	231.02	99.34	31.84	-2.02	323.49
120		cataclasite	292 cm	0.86	16.28	46.51	55.14	69.33	-56.35	140.18	46.17	161.85	82.99	43.60	-1.96	168.65
119		cataclasite	270 cm	0.76	31.56	94.71	58.91	71.30	-0.36	56.58	223.08	119.49	44.49	28.2	-2.32	809.23
118	DFDP-1A	cataclasite	135 cm	0.93	7.96	-7.16	41.48	29.32	-58.06	121.40	23.11	103.53	26.07	18.35	-0.84	100.06
117		cataclasite	87 cm	0.76	32.43	111.89	62.06	48.71	-63.69	105.81	240.66	210.11	55.75	19.21	-2.06	844.08
116		cataclasite	25 cm	0.64	55.21	430.81	121.78	128.28	-80.75	171.74	1005.22	420.20	145.97	38.40	-3.46	910.75
115		gouge	0 cm	0.88	13.47	31.62	60.35	33.33	-52.22	112.06	49.25	79.97	26.19	15.18	-1.04	318.2
132		cataclasite	70 cm	0.84	19.03	219.01	3.37	120.21	63.20	-69.56	188.46	339.03	155.83	31.04	-1.78	70.37
124		cataclasite	25 cm	0.79	26.61	206.41	-6.04	37.69	34.33	-81.32	261.79	199.33	96.43	24.25	-1.99	564.10
125_1	Waikukupa Thrust	cataclasite	8 cm	0.82	21.60	165.08	-8.80	54.27	23.45	-73.69	241.94	212.93	88.31	18.58	-1.56	407.74
131_2		gouge	2 cm	0.72	38.66	324.29	71.86	108.28	-37.54	43.89	806.52	209.13	137.09	35.44	-2.85	675.78
131_1		gouge	0 cm	0.56	78.51	853.23	83.21	112.72	-50.47	56.27	2786.97	223.18	157.09	37.71	-3.99	763.04
133		gravel	-10 cm	0.92	9.28	146.97	32.00	83.50	8.09	-2.19	74.89	124.01	85.94	23.48	-1.11	13.84
127_3	Martyr River	cataclasite	2 cm	1.05	-4.44	-43.42	26.05	-21.40	-9.39	189.57	-25.18	-43.95	-43.67	-15.12	5.29	128.73
127_4		gouge	0 cm	1.09	-8.54	-49.46	-1.42	-39.56	-20.16	138.65	-71.32	26.24	47.15	33.13	8.31	79.31

a) Datum to calculate distance to PSZ refers to center of PSZ at Martyr River, Havelock Creek and the DFDP-1A borehole and to the contact between PSZ and footwall at Waikukupa Thrust and Gaunt Creek.

b) Fe₂O₃ is total Fe content.